Weather and Climate Extremes 36 (2022) 100446

Contents lists available at ScienceDirect

Weather and Climate Extremes

journal homepage: www.elsevier.com/locate/wace

# Typhoon strength rising in the past four decades

Ravi Shankar Pandey [a,b], Yuei-An Liou [a,b,*]

[a] Center for Space and Remote Sensing Research, National Central University, No. 300, Jhongda Rd., Jhongli District, Taoyuan City, 320317, Taiwan, ROC
[b] National Museum of Marine Science and Technology, No. 367, Beining Rd., Zhongzheng Dist., Keelung City, 202010, Taiwan, ROC

ARTICLE INFO

*Keywords:*
El Niño Southern oscillation
Sea surface temperature
Sea surface temperature anomaly
Cyclogenesis

ABSTRACT

Quantitative and climatological analysis on the tracks and cyclogenesis locations of all 77 typhoons that hit Taiwan in the last 40 years (1977–2016) during typhoon season (May to November) is carried out. Ten pathways of all typhoons that hit Taiwan are detected with almost 1.9 typhoons per year. 53% of typhoons hit Taiwan from the East direction, typically (78%) only from the Philippine Sea. Typhoons from the West uniquely survive the longest hours with the highest sinuous tracks, often (59%) only from the South China Sea. Typhoons striking Taiwan from the East are the most intense whereas from the West the least intense. The Fisher's Exact and Chi-square ($\chi 2$) tests also establish that the sinuous nature of the tracks of typhoons is more responsible for the longer survival of typhoons ($r = 0.67$) than its strength. 26% more cyclogenesis is detected during the warm phase of El Niño Southern Oscillation (ENSO) than in the cold phase, which is also gradually rising in the last 4 decades. A 35% crucial growth in the strength of typhoons that hit Taiwan is observed by 0.4–0.7 °C rise in the Sea Surface Temperature (SST) in all four responsible oceans during the last 40 years (1977–2016). The role of the El-Niño epochs is found very crucial for the major SSTA changes during the typhoon season. The climatological analysis is fully consistent with statistical findings and leads to global warming as the major cause of the rising strength of typhoons that hit Taiwan during the study period.

## 1. Introduction

Typhoons are one of the most destructive natural phenomena that are responsible for the great loss of life and destruction of property worldwide. Most of the damages arise from secondary typhoon-associated events like heavy rain-triggered floods and/or landslides, and storm surges than the primary typhoon-associated events like strong wind and heavy rain (Peduzzi et al., 2012; Janapati et al., 2019; Nguyen et al., 2019). Among all seven typhoon prone ocean basins in the world, the North West Pacific (NWP) Ocean basin, which includes many major marginal seas like the South China Sea, Eastern China Sea, Philippine Sea, Sea of Japan, Coral Sea, Tasman Sea, and the Sea of Okhotsk, alone accounts for one-third (30%) of all typhoons on the whole globe since 1970. Over a 40-yr (1977–2016) period, the NWP basin produced an average of 24 typhoons per year, which is the maximum among all typhoon-prone ocean basins of the world (Pandey and Liou, 2020a, b, c). Taiwan ranks as number seventh country globally to be hit by typhoons since 1970 along with setting a record of receiving the wettest known typhoon (Typhoon Morakot, 2009) in the NWP basin (NOAA Hurricane Research Division, 2010). Taiwan receives on average 1.8 typhoon landfalls each year (Zhang et al., 2009).

Globally speaking, the strength of typhoons is rising (Emanuel, 2005; Webster et al., 2005; Knutson et al., 2008). A 10% increase in the strength of the typhoons of the NWP since 1970 is noticed due to increased Sea Surface Temperature (SST) (Mei et al., 2015). Pandey and Liou (2020a) recently showed that the frequency of typhoons crosses double (391) by particularly adding intense typhoons in the eastern side of the NWP basin, in the case of the warm phase of El Niño Southern Oscillation (ENSO) in comparison to the cold phase (118). Recent studies identify a crucial role of southwest air-flow and northwest cold air mass in summer and winter seasons, respectively, in escalating the typhoons of the NWP basin up to a level of converting them into more intense Super-Typhoons (STY) (Lee et al., 2017; Liou et al., 2018; Pandey et al., 2021). The recent years 2013–2016 recorded the maximum average frequency of STYs with 7 STYs per year along with 5 months with double-STY events, which is an alarming situation for the NWP region (Pandey et al., 2021). These investigations by Pandey et al. (2021) were found crucial for the NWP and thus reported by a recent

* Corresponding author. Center for Space and Remote Sensing Research, National Central University, No. 300, Jhongda Rd., Jhongli District, Taoyuan City, 320317, Taiwan, ROC.
*E-mail addresses:* babaravi1988@g.ncu.edu.tw (R.S. Pandey), yueian@csrsr.ncu.edu.tw (Y.-A. Liou).

https://doi.org/10.1016/j.wace.2022.100446
Received 4 June 2021; Received in revised form 8 February 2022; Accepted 22 April 2022
Available online 9 May 2022

publication of Eos, Transactions American Geophysical Union in the sub-topic of "Rising Super Typhoons" and the main topic of "Typhoons Getting Stronger, Making Landfall More Often", highlighting the major role of southwest airflows and northwest cold air masses in intensifying the STYs in summer and winter seasons, respectively (Hornyak, 2020; Pandey et al., 2021). Note here that a typhoon is called a STY if its maximum (01-min mean) sustained wind reaches ≥113 knots. This intensification of typhoons in the NWP region also supports the interaction between two typhoons. The interaction between typhoons is typically known as the Fujiwhara effect. The Fujiwhara effect makes prediction rather challenging for models. A recent study showed that interaction between two typhoons (Parma and Melor, 2009) in the NWP basin can cause very heavy unexpected damage due to less accurate predictions (Liou and Pandey, 2020). Moreover, 7 out of 30 STYs during 2013–2017 were found involved in causing the Fujiwhara effect in a recent analysis (Pandey et al., 2021). Recently Eos reported a unique formula developed by Liou et al. (2016) to catch the probability of significant interaction between hurricane Laura and tropical storm Marco (August 2020) in the Gulf of Mexico. It was published in Eos as a sub-topic of "A Rare Coexistence" under the main topic of "Storms Interact but Rarely Merge into Bigger Tempests" (Kornei, 2020). In addition, a recent study also showed that the swelling strength of typhoons in the NWP basin is also increasing the curviness (sinuosity) of their tracks, which further assists them to survive longer covering rather longer distances and hence creating more damage (Pandey and Liou, 2020a). STY Haiyan (2013) with the maximum (10-min mean) sustained wind of 230 km/h was the deadliest STY of the NWP region in recent years. Whereas, typhoon Morakot (2009) was the heaviest rain-producing typhoon ever in the NWP basin and the deadliest typhoon to impact Taiwan in recorded history. Typhoon Morakot caused many provinces of Taiwan flooded by record-breaking heavy rain, costing 673 deaths and roughly US$3.3 billion loss (Morakot Post-Disaster Reconstruction Council Report, 2010). Thus, the researches focus on understanding the fluctuating Spatio-temporal patterns of strength and nature of track of typhoons that reach any individual country, which is very crucial for preparedness by disaster mitigation-related agencies to reduce loss.

Due to Taiwan's position on the map, the country is partially exposed to all kinds of track following typhoons ranging from the most straight to the most sinuous or recurvature tracks. For clarification, when curviness or sinuosity in the tracks of typhoons increases, it also increases their chance of taking recurvature due to the application of Coriolis force. Moreover, Taiwan receives typhoons from three directions, East, West, and South from four nearby marginal oceans of NWP namely the Philippine Sea, South China Sea, Eastern China Sea, and North Pacific Ocean. Thus, the typhoons that strike Taiwan follow many pathways with varying typhoon parameters to reach the country (Chang et al., 2018). There are several recent studies on Taiwan correlating the increasing strength and frequency of intense typhoons hitting Taiwan to the rising SST anomalies (SSTA) over the equatorial western and central Pacific (Tu et al., 2009, 2011; Mei and Xie, 2016). Hence, the detailed long-term (last 40-years) quantitative analysis on the nature of tracks and strength of typhoons along with the long-term climatological analysis on cyclogenesis locations by measuring SSTA for all the typhoons that hit Taiwan, can provide very vital information for disaster management agencies of the country. In addition, distributing the typhoon cases by typhoon pathways, the direction of hitting Taiwan, El Niño Southern Oscillation (ENSO) phases at the time of cyclogenesis, and oceans of cyclogenesis, can be crucial to enhance our understanding further.

## 2. Aims

The current paper first aims to detect all typhoon pathways through which typhoons reach Taiwan by the available 40-year data from 1977 to 2016. Then it aims to statistically investigate the fundamental typhoon parameters like frequency, strength, track length, survival time, etc. along with a few new parameters like track sinuosity, the direction of hitting Taiwan, ENSO phases at cyclogenesis, oceans of cyclogenesis, the month of cyclogenesis, etc. Note that all the abovementioned parameters are also checked for their decadal variation. Moreover, the paper aims to conduct a climatological investigation based on cyclogenesis positions of typhoons over four oceans, namely the Philippine Sea, South China Sea, Eastern China Sea, and North Pacific Ocean by measuring Decadal, 5-yearly, yearly, ENSO-phase-wise, and monthly-wise Sea Surface Temperature Anomalies (SSTAs) over the 1977–2016 timeframe with a base year duration of 30 years (1941–1970). Note that all SSTA was also measured for the whole global ocean for comparing purposes. Maximum wind speed and minimum pressure map for representing the strength of all typhoons during study years inside Taiwan are made to aid in analysis. Finally, the results of both climatological and statistical quantitative analysis are correlated for an overall understanding of the nature of tracks and cyclogenesis locations of all typhoons that hit Taiwan in the last 40 years (1977–2016).

## 3. Study region

Typhoons that hit Taiwan have cyclogenesis in four nearby oceans, which are marginal Seas of the NWP basin, namely the Eastern China Sea, Philippine Sea, South China Sea, and North Pacific Ocean. Fig. 1 shows the respective boundaries of the study oceans.

For clarification, the North Pacific Ocean starts from the most west boundary of the Philippine Sea. In some research, both the Philippine Sea and North Pacific Ocean are considered as one NWP Ocean. According to the International Hydrographic Organization (IHO) (1953), the Philippine Sea is the portion of the Northwest Pacific Ocean that is off the coasts of the Philippine Islands. Besides the above shown four oceans, the entire global ocean also has been used for comparing SSTA with the other oceans. All the above-shown oceans' boundaries are adopted from the IHO (1953), provided by the online link https://www.marineregions.org/gazetteer.php?p=details&id=4332.

## 4. Data and methods

### 4.1. Data extraction and sorting

This paper uses primarily two types of data for investigation, namely typhoon data and SST data. The details about each kind of data are shown below:

(1) The original data of typhoons with individual typhoon name, minimum central pressure, maximum wind speed (10-min mean),

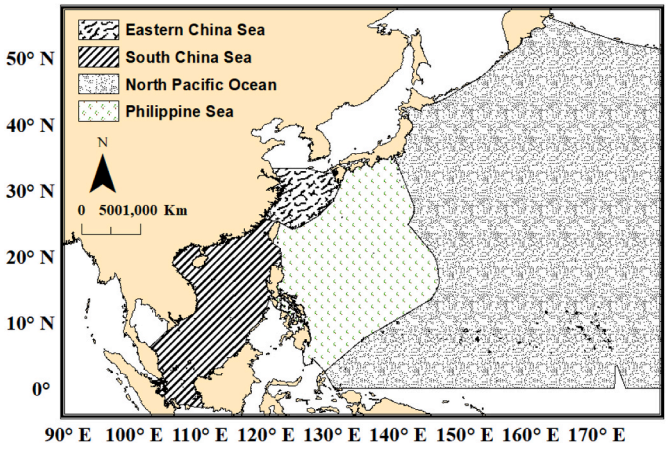


**Fig. 1.** Study ocean regions, namely the Eastern China Sea, Philippine Sea, South China Sea, and North Pacific Ocean.

time stamps, latitudes, and longitudes are provided by International Best Track Archive for Climate Stewardship (IBTrACS) database (https://www.ncdc.noaa.gov/ibtracs/index.php), which is available freely in the public domain for research activities by the US National Oceanic and Atmospheric Administration (NOAA). For the NWP Ocean zone, the IBTrACS dataset contains 1 695 typhoon data collected by the Regional Specialized Meteorological Center–Tokyo (RSMC–Tokyo) center of the Japan Meteorological Agency (JMA) from 1951 to 2017. The dataset sorting is needed to make it smooth for statistical analysis and improve the quality of investigation. Pandey and Liou (2020b, c) used some useful steps to increase the quality of typhoon data for the NWP basin. The steps are shown below: (a) *Time frame correction for accuracy:* Before 1977, the NWP basin typhoon data did not solely depend on satellites, so its accuracy was questionable (Song et al., 2010). Also, only since 1977, the maximum wind speed was provided along with full utilization of the Dvorak technique in data by RSMC–Tokyo (Dvorak, 1972, 1973; Song et al., 2010; Schreck et al., 2014). The dataset had only two cases from 2017, which was not enough for the analysis for that year. Hence, an overall of 714 such data was excluded along with one individual case of only one datapoint; (b) *tropical cyclones*: 22 such typhoon cases whose cyclogenesis locations were beyond the range of 0°–30° N were also excluded as they are not tropical cyclone cases; (c) *Timestamp smoothness*: Dataset had mostly 6-hourly, along with few 3-hourly and 1-hourly datapoints. To smooth the whole dataset for statistical purposes all 3-hourly and 1-hourly datapoints were removed; (d) *Immature datapoint exclusion:* Datapoints that belong from typhoon depression immature stages during cyclogenesis and cyclolysis processes when maximum wind speed ≤35 knots, create misunderstanding and are inappropriate for measuring the track of a typhoon for statistical analysis. All such datapoints were removed from the cases. Thus, a final dataset containing 959 sorted and improved typhoon cases for the whole NWP basin during 1977–2016 is kept available for public use in form of GIS-compatible files by the online Mendeley repository with data identification number: https://doi.org/10.17632/3927f6gm72.1 and detailed data explanation is available in Pandey and Liou (2020c). Note here that cyclogenesis is the beginning or formation process of a typhoon/cyclone before achieving 35 knots maximum wind speed for the first time in its life journey. Whereas, cyclolysis is the decay process of a typhoon/cyclone after achieving 35 knots maximum wind speed for the last time in its life journey. Similarly, cyclogenesis and cyclolysis locations are those places on the map where a cyclone/typhoon achieves its 35 knots maximum wind speed for the first and last time during its journey, respectively. This current paper further filters the data for selecting the typhoons that hit Taiwan with a next step: (e) *typhoons that hit Taiwan*: an overall of 77 typhoons of interest are found with an average of 1.9 typhoon cases per year, which is slightly more than previously found 1.8 typhoons per year (Zhang et al., 2009).

(2) This paper uses two monthly SST datasets as explained below: (a) *monthly Optimum Interpolation (OI) Sea Surface Temperature (SST) version-2 dataset*: This dataset is constructed by using in situ (ships, buoys, and Argo floats) and satellite SST's including SST's simulated by the sea-ice cover on a regular global one-degree (1°) grid. The final analysis is completed by filling spatial gaps by interpolation and bias adjustment of satellite and ship observations by using method of Reynolds to compensate for the platform differences and sensor biases (Reynolds et al., 2002). The weekly OI-SST V2 fields to daily fields are converted into monthly fields by linear interpolation and averaging the daily values over a month. The dataset contains monthly averaged SST for the whole global ocean from December 1981 to May 2020; and (b) *monthly Centennial* in situ *Observation-Based Estimates (COBE) SST version-2 dataset*: This dataset is constructed by using in situ SST and sea-ice concentrations as a sum of daily changes, interannual changes, and trend on a regular global one-degree (1°) grid. The final step is completed by using theory-based analysis errors as a measure of reliability, an ice-SST relationship equation to produce SST data from the observed sea ice concentrations, and biases of individual SST measurement types for a homogenized long-term time series of global mean SST. The daily COBE-SST V2 fields are converted into monthly fields by averaging. The dataset contains monthly averaged SST for the whole global ocean from January 1850 to December 2019. The COBE SST dataset originally belongs to the Japan Meteorological Agency (JMA). Both OI-SST V2 and COBE SST V2 datasets are freely accessible by the online website at https://psl.noaa.gov/, which is made available by the Physical Sciences Laboratory (PSL) of NOAA. This paper uses both SST datasets to cover the entire 40-year study period of 1977–2016 along with the 30-year base period of 1941–1970.

### 4.2. Typhoon track sinuosity index

Terry and Gienko (2011) showed that the curviness of tracks of typhoons is directly associated with their survival time and distance coverage during their life journey. A new index was introduced as a measure of the level of curviness of the typhoon tracks for the detailed comparison with typhoon fundamental parameters (Terry and Gienko, 2011). The index was known as the typhoon track Sinuosity Index (SI) and was tested in various ocean basins (Terry and Gienko, 2011, 2018; Terry et al., 2013; Terry and Kim, 2015). Recently, we investigated the SI of all typhoons of the NWP basin in 4 decades and correlated it with the other parameters. The simple formula to measure the sinuous nature of tracks is found by dividing the total geodesic track length of each typhoon from the direct geodesic distance between its cyclogenesis and cyclolysis locations on the map. Note here that the geodesic distance is the shortest route distance between two points on earth treating the Earth as an oblate spheroid. The typhoon track SI was made using the track sinuosity values as explained above. The normalization of typhoon track sinuosity values by measuring the SI reduces the skewness in data and makes it more appropriate for statistical analyses by increasing the contrast between values (Terry and Gienko, 2011; Pandey and Liou, 2020a). The SI formula is as given below:

$$\mathrm{SI} = \sqrt[3]{S-1} \times 10 \quad (1)$$

where,

SI = track SI value for each typhoon
S = measured track sinuosity value for each typhoon

By equation (1), a typhoon with a perfectly straight track will have a SI value of zero (0)

The typhoon track SI values are utilized in this paper as a measure of the level of curviness of typhoon tracks for all 77 typhoons individually that hit Taiwan during 1977–2016. Geodesic track length, and direct geodesic distance between cyclogenesis and cyclolysis locations on the map for the case of each typhoon, are also used for statistical analysis in the paper.

### 4.3. Statistical investigation technique

Statistical investigations on the fundamental typhoon parameters like frequency, strength, track length, survival time, etc. along with a few new parameters like track sinuosity, the direction of hitting Taiwan, ENSO phases at cyclogenesis, oceans of cyclogenesis, the month of cyclogenesis, etc. are executed. Decadal variations of all the above-mentioned parameters are also checked for spotting patterns. The Chi-

square ($\chi 2$) test for independence is used to determine if there is any significant relationship between two categorical variables from a single population. It was used in the previous studies for finding any longitudinal and latitudinal significant differences in the typhoon-related parameters (Terry and Gienko, 2011; Terry and Kim, 2015; Pandey and Liou, 2020a). However, when few of the expected values are small, Fisher's exact test is more accurate than the Chi-square ($\chi 2$) test of independence because it does account for the zero value in a cell. As the number of cases (77) of typhoons that struck Taiwan in the last 40 years is small, it has a great possibility to have sometimes zero (0) value in a typhoon parameter class cell. It is a well-established fact that, when any parameter class cell value (i.e., sample size) is less than 5, the reliability of the results of the Chi-square test drops. Hence, for the current paper, both statistical tests are applied. The traditional Fisher's exact test is only computationally realistic for $2 \times 2$ tables, but the Freeman-Halton test extends the Fisher's Exact test to the m x n setting.

In the current paper, both Fisher's Exact and Chi-square ($\chi 2$) tests were executed for checking if there is any statistically significant difference both longitude- and latitude-wise in each typhoon-related parameter-class (sinuosity, strength, direction, and ENSO) based on its cyclogenesis position.

### 4.4. ENSO-phase detection

The Multivariate ENSO Index (MEI) is widely used in typhoon-related research for separating typhoons in warm and cold phases of ENSO based on their respective months of cyclogenesis (Astier et al., 2015; Jien et al., 2015; Pandey and Liou, 2020a). It was showed that the frequency of typhoons as well as the chance of rather intense typhoons increases during the warm phase of ENSO than the cold phase in the NWP based on MEI. A significant statistical correlation between the ENSO and tropical cyclone activity was found in the western area of the Pacific using MEI. While a non-linear reduction of tropical cyclone activity was seen over the Southwest Indian Ocean using MEI during strong ENSO cases (Astier et al., 2015). In general, MEI is considered a better representative of ENSO activities because it combines both oceanic and atmospheric variables (Wolter and Timlin, 2011).

Following the above, MEI is the time series of the leading combined Empirical Orthogonal Function (EOF) of five different variables. These variables are both atmospheric and oceanic such as sea surface temperature (SST), sea level pressure (SLP), meridional and zonal components of the surface wind, and outgoing longwave radiation (OLR) over the tropical Pacific basin (30°S-30°N and 100°E–70°W). The EOFs are measured for 12 overlapping bi-months like Dec–Jan, Jan–Feb, Feb–Mar, …, Nov–Dec, so that it reduces the effects of higher frequency intra-seasonal variability in order to create ENSO's seasonality. Hence, it can be considered the crucial technique for obtaining the real-time status of ENSO, which makes it important for a host of climate services. Other ENSO indices, except MEI, typically provide years with El Niño and La Niña, but are not suitable to provide intra-seasonal variability within a year or typhoon season. The combined effect of above mentioned five major environmental parameters, used to measure MEI, is heavily responsible for deciding typhoons' strength and frequency at any particular time in any region. Suitable conditions of MEI measuring parameters in any particular month can cause the amplified frequency of cyclogenesis in that individual month, the same is also noted by previous research in the NWP (Astier et al., 2015; Jien et al., 2015; Pandey and Liou, 2020a). For this paper, MEI values are extracted by the online site https://psl.noaa.gov/enso/mei/, which is kept to use freely by NOAA. Fig. 2 shows all ENSO values during the study period (1977–2016). Typhoons are separated in warm and cold phases of ENSO if the MEI values are $> +0.5$ and $< -0.5$, respectively.

### 4.5. SST data analyses technique

The Optimum Interpolation (OI) Sea Surface Temperature (SST) version-2 and COBE SST version-2 datasets are used to extract each month data of typhoon season from May to November for two-time durations, one from 1977 to 2016 (40-years) for the study period and another from 1941 to 1970 (30-years) for the base period. The analysis details are as given below:

(a) *For month-wise climatological investigations:* the raster average of all data images from the same typhoon season month (among May to November) is measured individually over the 1977–2016 study period with 1941–1970 as the base period, and separately for each of 4 decades of the study period.
(b) *For 10-yearly, and 5-yearly climatological investigations*: typhoon seasonal-averaged raster data are formed by averaging all months' data from May to November for the study period and base period, and separately for each 10-yearly, and 5-yearly study period.
(c) *For year-wise climatological investigations:* typhoon seasonally (from May to November) averaged raster data of each study year from 1977 to 2016 is measured separately. It is compared with the raster average for all typhoon season months (from May to November) of the entire base period (1941–1970).
(d) *For ENSO phase-wise climatological investigation:* at first, all cases of typhoons are separated into warm and cold phases of ENSO based on their month of cyclogenesis and Multivariate ENSO Index (MEI) values as described in Section 4.4. Then, all cases are averaged for all available typhoon season months and kept decade-wise along with for the whole study period. Note here that ENSO-phase based typhoons do not necessarily belong to all months of typhoon season (May–November) as shown below: (i) ENSO warm phase months: *August, and September for D1:*

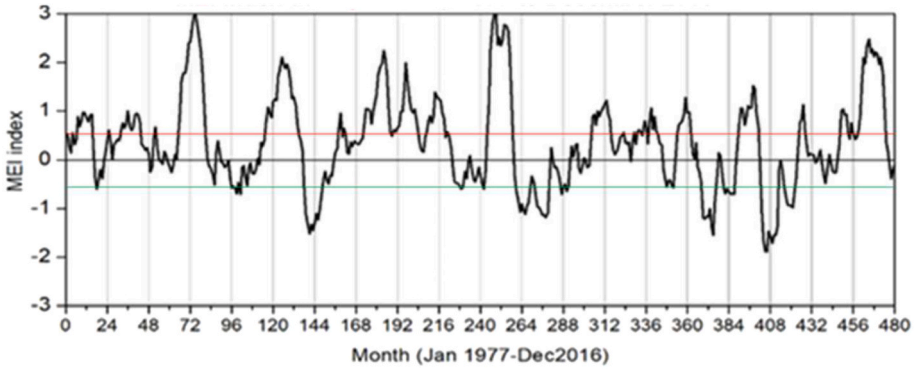


**Fig. 2.** Multivariate ENSO Index values over the study period from 1977 to 2016. The X-axis represents each month from January 1977 to December 2016; n = 480. Red and green lines represent the separation baseline of ENSO phases which is $> +0.5$ and $< -0.5$ MEI values for separating typhoons in warm and cold phases of ENSO, respectively. (For interpretation of the references to color in this figure legend, the reader is referred to the Web version of this article.)

*2007–2016; July, August, September, October, and November for D2: 1997–2006; July, August, and September for D3: 1987–1996; June, July, August, and September for D4: 1977–1986; June to November for the whole study period,* and (ii) ENSO cold phase months: *July, August, September, and October for D1; July, August, and September for D2; May, July, and September for D3; June, July for D4; May to October for the whole study period.* Hence, ENSO-phase wise separated data is averaged for all available months of each of four decades and also for the whole study period.

Finally, Sea Surface Temperature (SST) Anomalies (SSTA) are measured based on variations of SST between study and base year raster data for all the above cases. Note here that in the ENSO-phase based climatological investigations, for all available month cases, the very similar months of the entire base year period are used to measure SSTA for consistency of investigation. A similar technique was adopted by James et al. (2006) for detecting SST variation during the study period of 2001–2005 with a base period of 1951–1980 by measuring SSTA.

### 4.6. Typhoon strength inside Taiwan

Although the focus of the paper is to investigate typhoons' track and cyclogenesis locations of typhoons that hit Taiwan, yet for a complete understanding of the strength of these typhoons inside Taiwan during these 40 years study period and also to correlate it with the overall results, two typhoons maps: (1) *maximum wind speed* and (2) *minimum central pressure*, are formed. Their methodologies are presented below:

The eye of a typhoon is nearby circular from the center at any particular time. It is also the circular zone of minimum pressure surrounded by an eyewall. An eyewall is the rounded ring shape made by clouds around the eye possessing zone of maximum speed winds in the typhoon (Smith, 1980). The distance from the center of the typhoon to the eyewall is known as the Radius of Maximum Wind (RMW). The average value of RMW is around 47 km using the observations based on several hurricanes with their central pressure between 909 and 993 hPa (Hsu and Yana, 1998). As the final refined IBTrACS dataset used in this paper provides a 6-hourly maximum wind speed and the minimum central pressure of typhoons that hit Taiwan during 1977–2016. The frequency of datapoints is less, so at first, by linear interpolations, assuming the homogeneous acceleration of both the above-mentioned typhoon parameters between any two successive datapoints of a typhoon, we have generated ten (10) more datapoints between all two successive datapoints of each typhoon. Then, we formed the ring at RMW and a circular area under RMW, both around the center of each typhoon representing maximum wind speed and minimum central pressure zones, respectively. This technique of confining typhoon strength up to the radius of maximum wind speed of typhoons is fairly suitable for a typhoon in motion following any particular track. Note here that RMW is taken as 0.5° (around 55.5 km) in ESRI ArcGIS 10.5 software equally for all typhoon cases and the Inverse Distance Weighting (IDW) interpolation technique is used at every created typhoon datapoint. Finally, using all results, the spatial mean of all 77 typhoon cases is measured to draw the maximum wind speed and the minimum central pressure map of Taiwan. These maps represent the strength of typhoons during the entire study period inside Taiwan.

## 5. Results and discussion

### 5.1. Typhoon pathways

Taiwan receives typhoons from many sides of the country following various routes, based on the ocean of cyclogenesis, the season of cyclogenesis, and the existing environmental conditions (Chang et al., 2018). Pandey and Liou (2020a) showed that Taiwan's position on the map makes it exposed to all kinds of tracks following typhoons ranging from the most straight to recurvature making most sinuous tracks of typhoons in the NWP basin. Chang et al. (2018) identified seven pathways of typhoons affecting Taiwan during 1981–2015 based on the data from the Typhoon database of the Central Weather Bureau (CWB) of Taiwan. However, the CWB of Taiwan classified typhoon events into nine typhoon pathway categories based on data from 1979 to 2018. Although, for clarification, all these previously created typhoon pathways were not necessarily for the typhoons that surely did landfall on Taiwan or hit the country, but rather broadly represented typhoons that affected Taiwan's weather by their presence even if they just passed nearby without contacting the land of the country. The current paper tries to identify and analyze all typhoon pathways during the study period (1977–2016) for the typhoons that hit Taiwan. Fig. 3 shows the different sets of tracks of typhoons of interest during 1977–2016.

The typhoons that hit Taiwan are originated from four marginal oceans of the NWP namely the Philippine Sea, the South China Sea, the Eastern China Sea, and the North Pacific Ocean based on the data from 1977 to 2016 (Fig. 1). The details about the boundaries and respective areas of these oceans are discussed in Section 3. Fig. 3 provides an overall of ten (10) typhoon pathways of typhoons of interest during 1977–2016. Typhoon pathways 1 and 2 belong to the maximum frequency of typhoons (around 18% each) and numbering in typhoon pathways (1–10) is done according to their decreasing frequency of typhoon cases that hit Taiwan during 1977–2016 (Fig. 3). Fig. 4 shows the cyclogenesis and cyclolysis locations of all typhoon pathways as detected in Fig. 3 above.

Table 1 provides the frequency, direction to enter Taiwan, average minimum pressure, ocean and month of cyclogenesis, average survival duration, track length, and average track Sinuosity Index (SI) values of all typhoons that hit Taiwan over 40 years categorized in different pathways.

Table 1 reveals that the top five (5) most frequent typhoon pathways together account for literally three fourth (75%) of all typhoons crossing over Taiwan in the past 40 years (1977–2016). Also, among these top five most frequent typhoon pathways, most of these typhoons (around 66%) chose to enter from the east (East-south) direction into Taiwan. The Philippine Sea dominates with around 76% of all typhoons in the top chart of the five most frequent typhoon pathways to Taiwan. Typhoons of pathway 1 with an average minimum pressure of 941.4 hPa are the most intense among all 10 typhoon pathways of Taiwan. Fig. 5 symbolically represents the average position of all typhoon pathways over Taiwan that hit the country during 1977–2016.

Chang et al. (2018) spotted six (6) out of seven (7) typhoons pathways that hit Taiwan directly during 1981–2015, whereas, CWB showed four (4) such typhoon pathways where typhoons belonging from them will definitely hit the land of Taiwan from the data over 1979–2018. Note here that the current paper focuses only on the typhoons that hit the land of Taiwan and does not account for those that just pass nearby the land affecting weather in Taiwan. Although the distribution of typhoons based on pathways alone reduces the frequency of typhoon cases to be analyzed in each pathway, the other kinds of categories like the direction of typhoons to hit Taiwan, etc., are also needed as vital information for a better analysis.

### 5.2. Direction-wise distribution

Taiwan obtains typhoons broadly from the three directions, East, West, and South if we consider only the typhoons that hit Taiwan. Fig. 6 classifies pathways of typhoons in terms of their respective directions to strike Taiwan during 1977–2016.

As it can be seen in Fig. 6 that the directions of pathways are having a little tilt to other directions as well thus not literally belong to only East, West, or South directions. Table 2 provides detailed statistical information about all typhoons to Taiwan classified in terms of their respective directions.

Fig. 6 and Table 2 reveal that more than half (53%) of all typhoons hit Taiwan from the East direction, while the rest one-fourth (25%) from

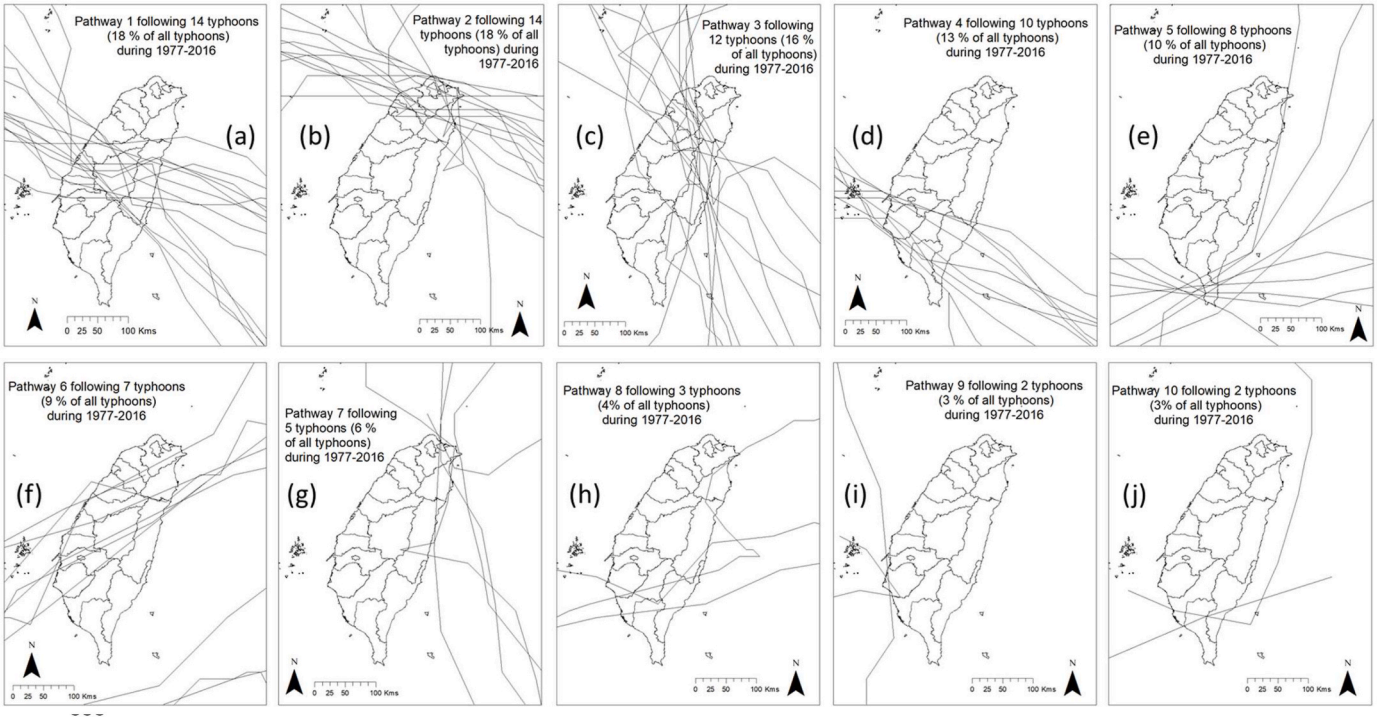


**Fig. 3.** Tracks, frequency, and percentage of typhoons following different pathways to hit Taiwan during 1977–2016.

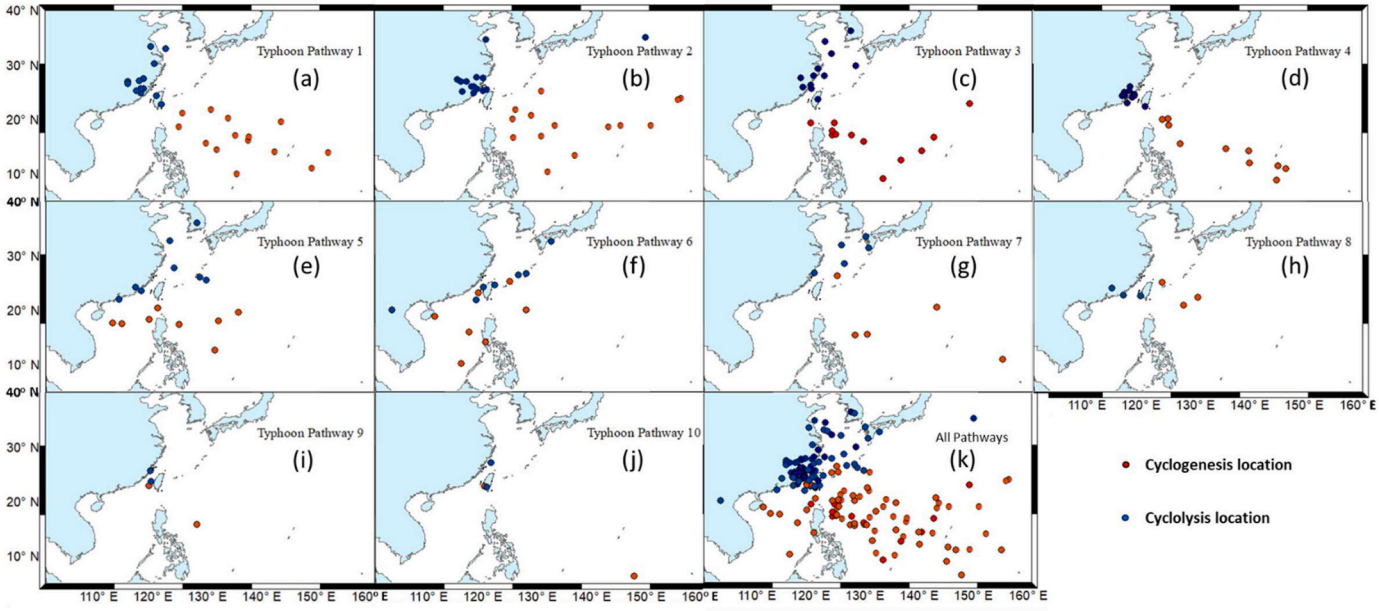


**Fig. 4.** Cyclogenesis and cyclolysis locations of all typhoons of different typhoon pathways that hit Taiwan during 1977–2016.

the South and around 22% from the West direction. Pathways 1, 2, 4, & 8 are associated with East directional typhoons striking Taiwan, whereas typhoon pathways 3, 7, & 9, and 5, 6, & 10 belong to South and West, respectively. The majority (93%, pathways 1, 2, and 4) of typhoons, which strike Taiwan from the East direction, are also having a Southwards tilt in their respective tracks. Following the above, the majority (89%, pathways 3, 7) of typhoons striking Taiwan from the South direction have an Eastwards tilt in their respective tracks. In comparison to the above both, all typhoons striking Taiwan from the West also possess a slight Southwards tilt in their tracks.

The Philippine Sea alone accounts for approximately 78% and 74% of all typhoons striking Taiwan from the East and South directions, respectively, while the South China Sea alone causes cyclogenesis to more than half (around 59%) of all typhoons hitting Taiwan from the West direction. There is a gradual but slight decadal decline in the frequency of the typhoons coming from the East side into Taiwan, while there is a zig-zag with alternate incline-decline patterns in the frequency of typhoons striking from the South direction to Taiwan. There is a decadal consistency in terms of the number of typhoons that hit Taiwan from the West direction during the studied four decades (1977–2016). Westerly striking typhoons are on average less intense but have the highest curves in their tracks, which helps them survive long hours than

**Table 1**
All typhoon parameters with their decadal variations classified in different typhoon pathways to Taiwan during 1977–2016; $n = 77$. Note here, D1: 2007–2016, D2: 1997–2006, D3: 1987–1996, and D4: 1977–1986.

| Typhoon Pathway over Taiwan | Percentage (frequency) | Direction | Average Minimum Pressure (in hPa) | Ocean of Cyclogenesis | Month of Cyclogenesis | Average Survival (hours) | Average Geodesic track length of typhoon (Kms) | Average Geodesic distance between Cyclogenesis and Cyclolysis locations (Kms) | Average Sinuosity value | Average Sinuosity Index value |
|---|---|---|---|---|---|---|---|---|---|---|
| 1 | **18% (14)** D1: 2; D2: 2; D3: 3; D4: 7 | **East** (east-south) | **941.4** (D1 ~ D4: 987.5, 925, 935, 935.7) | Philippine Sea (12), North Pacific Ocean (2) | June (1), July (3), Aug (7), Sept (3) | **142.2** (D1 ~ D4: 30, 162, 164, 9.4) | 2503.4 (D1 ~ D4: 592.3, 2887.8, 2736.2, 2839.9) | 2218.3 (D1 ~ D4: 577.7, 2781.8, 2606.4, 2359.6) | 1.12 (D1 ~ D4: 1.03, 1.03, 1.05, 1.20) | **4.29** (D1 ~ D4: 2.88, 3.17, 3.66, 5.27) |
| 2 | **18% (14)** D1: 4; D2: 6; D3: 1; D4: 3 | **East** (east-south) | **952.1** (D1 ~ D4: 960, 955.8, 970, 928.3) | Philippine Sea (11), North Pacific Ocean (3) | July (6), Aug (6), Sept (1), Oct (1) | **142.3** (D1 ~ D4: 70.5, 166, 144, 190) | 2641.1 (D1 ~ D4: 1378.3, 3216.6, 2705.0, 3152.3) | 2374.6 (D1 ~ D4: 1317.5, 2925.7, 2640.2, 2593.5) | 1.11 (D1 ~ D4: 1.05, 1.10, 1.02, 1.22) | **4.25** (D1 ~ D4: 3.42, 4.39, 2.91, 5.51) |
| 3 | **16% (12)** D1: 2; D2: 2; D3: 6; D4: 2 | **South** (south-east) | **954.2** (D1 ~ D4: 952.5, 977.5, 952.5, 937.5) | Philippine Sea (10), North Pacific Ocean (1), South China Sea (1) | June (2), July (5), Aug (1), Sept (4) | **125** (D1 ~ D4: 105, 138, 131, 114) | 2268.5 (D1 ~ D4: 2151.6, 2887.8, 2138.8, 2154.9) | 1827.9 (D1 ~ D4: 1888.1, 2373.3, 1719.1, 1548.7) | 1.23 (D1 ~ D4: 1.12, 1.22, 1.24, 1.30) | **5.53** (D1 ~ D4: 4.53, 5.86, 5.59, 6.01) |
| 4 | **13% (10)** D1: 2; D2: 2; D3: 4; D4: 2 | **East** (east-south) | **954.1** (D1 ~ D4: 950, 975, 966.5, 912.5) | Philippine Sea (7), North Pacific Ocean (3) | July (4), Aug (5), Sept (1) | **112.8** (D1 ~ D4: 168, 75, 81, 159) | 2202.2 (D1 ~ D4: 3480.7, 1885.1, 1616.7, 2411.5) | 2115.7 (D1 ~ D4: 3326.0, 1799.1, 1583.1, 2287.5) | 1.04 (D1 ~ D4: 1.05, 1.05, 1.02, 1.08) | **3.20** (D1 ~ D4: 3.59, 3.58, 2.44, 3.95) |
| 5 | **10% (8)** D1: 3; D2: 2; D3: 0; D4: 3 | **West** (west-south) | **961.9** (D1: 955, D2: 968.3, D4: 970) | South China Sea (4), Philippine Sea (4) | May (1), June (2), Aug (2), Sept (3) | **168.8** (D1: 122, D2: 200, D4: 168) | 2610.8 (D1: 2003.0, D2: 2585.3, D4: 156.8) | 1707.5 (D1: 1674.5, D2: 1236.4, D4: 2249.8) | 1.93 (D1: 1.19, D2: 2.97, D4: 1.41) | **7.39** (D1: 5.36, D2: 10.14, D4: 6.42) |
| 6 | **9% (7)** D1: 2; D2: 2; D3: 2; D4: 1 | **West** (west-south) | **980.4** (D1 ~ D4: 970, 980.5, 988.5, 985) | South China Sea (5), Philippine Sea (1), Eastern China Sea (1) | May (1), June (2), July (1), Aug (3) | **142.3** (D1 ~ D4: 306, 105, 48, 78) | 2274.7 (D1 ~ D4: 4974.4, 1716.4, 675.2, 1190.8) | 1130.1 (D1 ~ D4: 1513.0, 1302.8, 585.9, 1107.3) | 1.78 (D1 ~ D4: 3.25, 1.32, 1.11, 1.08) | **7.18** (D1 ~ D4: 12.66, 6.84, 3.53, 4.23) |
| 7 | **6% (5)** D1: 2; D2: 1; D3: 1; D4: 1 | **South** (south-east) | **960.0** (D1 ~ D4: 960, 950, 945, 985) | Philippine Sea (3), North Pacific Ocean (1), Eastern China Sea (1) | June (2), Sept (2), Oct (1) | **129.6** (D1 ~ D4: 93, 186, 228, 48) | 2838.9 (D1 ~ D4: 2487.2, 3608.1, 4808.9, 803.3) | 2128.1 (D1 ~ D4: 1925.0, 2395.2, 3602.7, 792.7) | 1.29 (D1 ~ D4: 1.29, 1.51, 1.33, 1.01) | **6.07** (D1 ~ D4: 6.54, 7.97, 6.94, 2.37) |
| 8 | **4% (3)** D1: 0; D2: 0; D3: 2; D4: 1 | **East** (east-north) | **956.7** (D3: 970, D4: 930) | Philippine Sea (2), Eastern China Sea (1) | Aug (1), Sept (2) | **172.0** (D3: 198, D4: 120) | 1856.2 (D3: 1922.9, D4: 1722.7) | 1076.7 (D3: 918.5, D4: 1393.1) | 1.96 (D3: 2.32, D4: 1.24) | **7.56** (D3: 8.25, D4: 6.19) |
| 9 | **3% (2)** D1: 1; D2: 0; D3: 1; D4: 0 | **South** (south-west) | **974.0** (D1: 950, D3: 998) | South China Sea (1), Philippine Sea (1) | July (2) | **60.0** (D1: 96, D3: 24) | 928.0 (D1: 1634.9, D3: 221.1) | 750.8 (D1: 1407.8, D3: 93.8) | 1.76 (D1: 1.16, D3: 2.36) | **8.26** (D1: 5.44, D3: 11.07) |
| 10 | **3% (2)** D1: 0; D2: 0; D3: 2; D4: 0 | **West** (west-south) | **965.5** (D3: 965.5) | South China Sea (1), North Pacific Ocean (1) | Sept (1), Nov ( | **84.0** (D3: 84) | 2354.0 (D3: 2354.0) | 1954.5 (D3: 1954.5) | 1.26 (D3: 1.26) | **6.29** (D3: 6.29) |

the other direction typhoons to hit Taiwan. Easterly striking typhoons are on average the most intense relatively, but their intensity possesses a decadal declining trend in the last 40 years along with decreasing survival hours and curviness in the tracks of the typhoons. Fig. 7 shows the mapping of three typhoon parameters i.e., ocean of cyclogenesis, strength, and direction to hit Taiwan based on the cyclogenesis locations of all typhoons during 1977–2016. Fig. 7 tells that around 77% of stronger typhoons (900–940 hPa) hit Taiwan from the East direction, while only 9% of stronger typhoons can strike Taiwan from the West, which is slightly less than 14% for typhoons hitting Taiwan from the South direction.

These results are just contrary to the prior research findings, which show that, with the increasing strength of typhoons, their track sinuosity or curviness should also increase (Terry and Gienko, 2011; Terry et al., 2013; Terry and Kim, 2015). Hence, these results are interesting as, for the typhoons striking Taiwan, the relationship between typhoon strength and track sinuosity is just reversed. The South China Sea is considered to have a big role in the reversal of this relationship as most of the Western typhoons come from there. As it is known that more sinuous track typhoons can survive longer hours and, thus, are more prone to create damage to the affected areas. Besides, the typhoons with more sinuous tracks are most of the time challenging for forecasting the prospective motion by the numerical weather prediction models. Thus, for Taiwan, the typhoons whose cyclogenesis is in the South China Sea need more attention for better forecasting. The South China Sea's environmental conditions are key factors behind creating more curvy tracks of typhoons, which consequently assist them to survive longer. Thus, there is a big need for investigation of the environmental conditions of the South China Sea. In general, the above discussion enhances the need for the ocean-wise investigation of typhoon cases that are

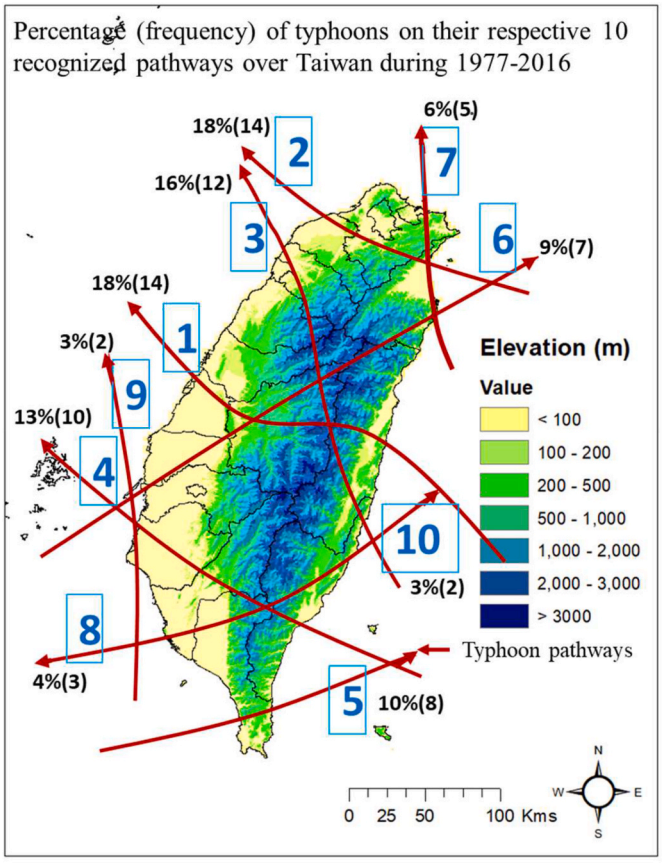


**Fig. 5.** Symbolic representation of all typhoon pathways belonging to typhoons that hit Taiwan with their respected frequencies during 1977–2016. Note here that the position of each typhoon pathway is based on the average fluctuation of all typhoons of that individual pathway while crossing Taiwan from the mid.

hitting Taiwan for detailed analysis ahead.

### 5.3. Decadal variations in typhoon strength

Fig. 8 shows the decadal variations in the strength of typhoons that hit Taiwan in the four decades based on their respective locations of cyclogenesis into the study oceans.

Fig. 8 tells that half (50%) of the strongest (900–920 hPa) and 43% of strong (921–940 hPa) typhoons belong from the current decade (F: 2007–2016), which can be potentially the impact of global warming. 80% of the current decade (2007–2016) typhoons are alone originated in the Philippine Sea. This indicates the importance of the Philippine Sea for Taiwan. It can be expected that, in the future, the cases of typhoons that originate from the Philippine Sea and later hit Taiwan, can gradually surge. Typhoon cases in the Eastern China Sea are only observed in the recent two decades (1997–2016). Half (50%) of the typhoons in the fourth and last (FL: 1977–1986) decade belong from the weaker typhoon categories (weak and weakest: 961-998 hPa). Also, 47% of typhoons from the third decade (T: 1987–1996) also belong to the weaker categories. In contrast, only 30% of typhoons from the current decade (2007–2016) belong to the weaker typhoon classes.

The average decadal strength of typhoons is 960. 8 hPa for 1977–1986, 960.1 hPa for 1987–1996, 961.2 hPa for 1997–2006, and 942.3 hPa for 2007–2016 with 18, 17, 22, and 20 typhoon cases, respectively. Hence, there is a 35.3% increase in the decadal-averaged strengths of typhoons from 1977 to 1986 to 2007–2016. Here, we have assumed that the mean sea-level pressure is 1013.25 hPa, which is adopted by the International Civil Aviation Organization (1993). Zhao et al. (2014) showed that the decadal increasing strength of typhoons in the NWP is due to a combined impact of variation in SST and vertical wind shear. The above result is concurrent with the previous results where the pattern of globally increasing strength of typhoons was detected (Emanuel, 2005; Webster et al., 2005; Knutson et al., 2008).

### 5.4. Ocean-wise distribution

The typhoons that strike Taiwan can have cyclogenesis in the four Seas namely the Philippine Sea, North Pacific Ocean, South China Sea, and Eastern China Sea. Table 3 provides detailed statistical information about all typhoons to Taiwan classified in terms of their ocean of cyclogenesis.

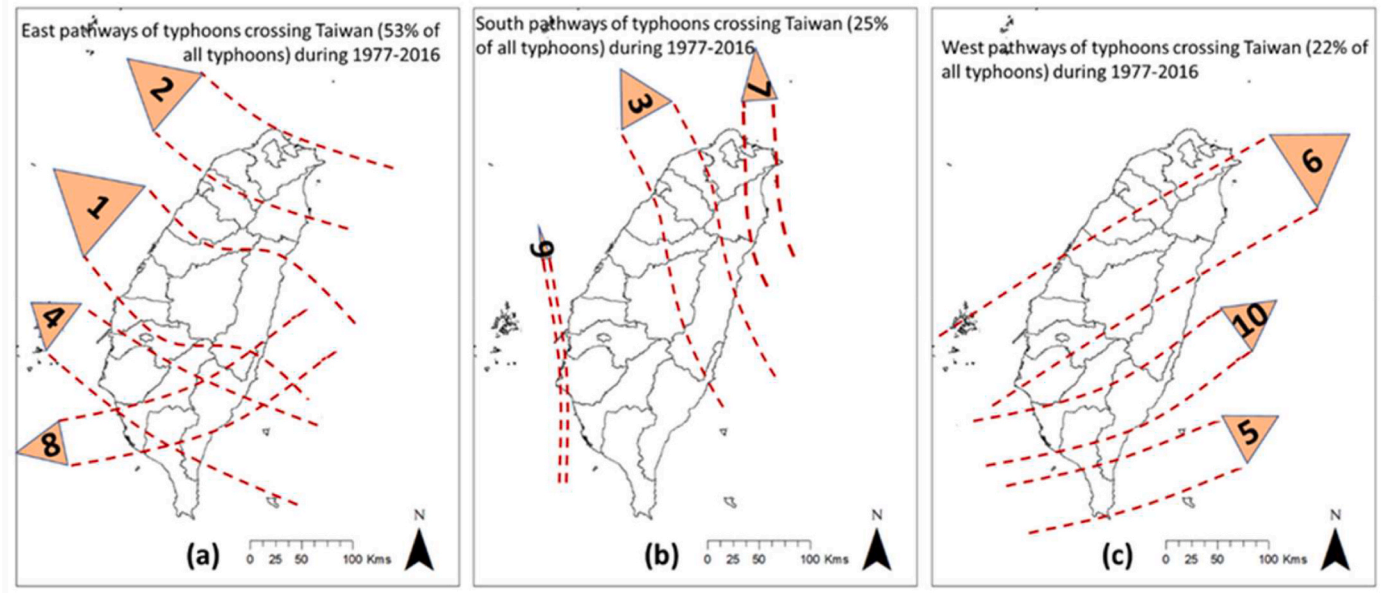


**Fig. 6.** Symbolic representation of pathways of typhoons classified in terms of their direction to hit Taiwan during 1977–2016.

**Table 2**
All typhoon pathways and parameters with their decadal variations classified in different directions of typhoons to hit Taiwan during 1977–2016; $n = 77$. Note here, D1: 2007–2016, D2: 1997–2006, D3: 1987–1996, and D4: 1977–1986.

| Typhoon Direction | Frequency (percentage) | Typhoon Pathway over Taiwan | Average Minimum Pressure (in hPa) | Ocean of Cyclogenesis | Month of Cyclogenesis | Average Survival (hours) | Average Geodesic track length of typhoon (Kms) | Average Geodesic distance between Cyclogenesis and Cyclolysis locations (Kms) | Average Sinuosity value | Average Sinuosity Index value |
|---|---|---|---|---|---|---|---|---|---|---|
| East | **41 (53%)** (D1: 8; D2: 10; D3: 10; D4: 13) | 1 (14), 2 (14), 4 (10), 8 (3) | **949.3** (D1 ~ D4: 964.4, 953.5, 958.1, 930) | Philippine Sea (32), North Pacific Ocean (8), Eastern China Sea (1) | June (1), July (13), Aug (19), Sept (7), Oct (1) | **137.3** (D1 ~ D4: 84.8, 147, 135.6, 163.4) | 2429.6 (D1 ~ D4: 1707.4, 2884.5, 2122.6, 2760.2) | 2163.1 (D1 ~ D4: 1634.7, 2671.6, 1862.9, 2328.1) | 1.16 (D1 ~ D4: 1.04, 1.08, 1.29, 1.19) | **4.25** (D1 ~ D4: 3.33, 3.98, 4.01, 5.19) |
| South | **19 (25%)** (D1: 5; D2: 3; D3: 8; D4: 3) | 3 (12), 7 (5), 9 (2) | **957.8** (D1 ~ D4: 955, 968.3, 957.3, 953.3) | Philippine Sea (14), North Pacific Ocean (2), South China Sea (2), Eastern China Sea (1) | June (4), July (7), Aug (1), Sept (6), Oct (1) | **119.4** (D1 ~ D4: 98.4, 154, 129.8, 92) | 2277.5 (D1 ~ D4: 2182.5, 3127.9, 2232.9, 1704.3) | 1793.5 (D1 ~ D4: 1806.8, 2380.6, 1751.4, 1296.7) | 1.30 (D1 ~ D4: 1.19, 1.32, 1.39, 1.21) | **5.96** (D1 ~ D4: 5.52, 6.56, 6.45, 4.80) |
| West | **17 (22%)** (D1: 5; D2: 4; D3: 4; D4: 4) | 5 (8), 6 (7), 10 (2) | **969.9** (D1 ~ D4: 961, 970.3, 977, 973.8) | South China Sea (10), Philippine Sea (5), Eastern China Sea (1), North Pacific Ocean (1) | May (2), June (4), July (1), Aug (5), Sept (4), Nov (1) | **147.9** (D1 ~ D4: 195.6, 172.5, 66, 145.5) | 2442.2 (D1 ~ D4: 3191.5, 2210.0, 1514.6, 2665.3) | 1498.8 (D1 ~ D4: 1609.9, 1123.0, 1270.2 1964.2) | 1.79 (D1 ~ D4: 2.02, 2.56, 1.18, 1.33) | **7.18** (D1 ~ D4: 8.28, 9.38, 4.91, 5.87) |

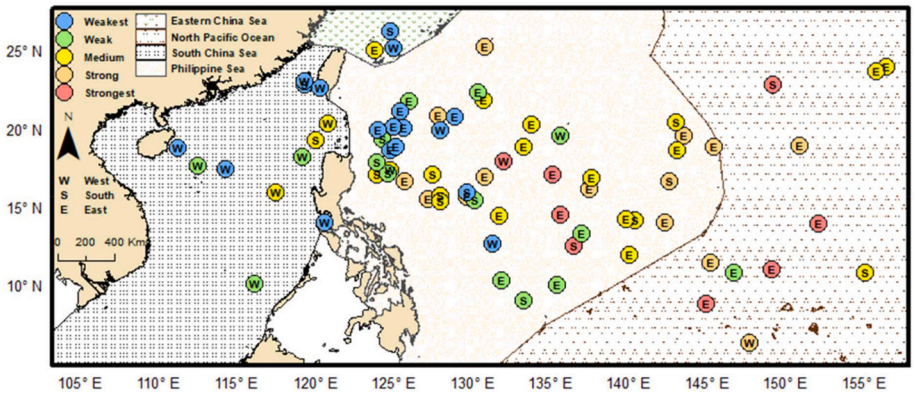


**Fig. 7.** Classification and mapping of the ocean of cyclogenesis, strength, and direction of typhoons to hit Taiwan based on cyclogenesis locations on the map for all typhoons during 1977–2016; n = 77. Note here that the maximum strength of typhoons is represented by colored dots on cyclogenesis locations. Colors red: strongest (900–920 hPa); orange: strong (921–940 hPa); yellow: medium (941–960 hPa); green: weak (961–980 hPa); and blue: weakest (981–998 hPa) typhoon strength class. (For interpretation of the references to color in this figure legend, the reader is referred to the Web version of this article.)

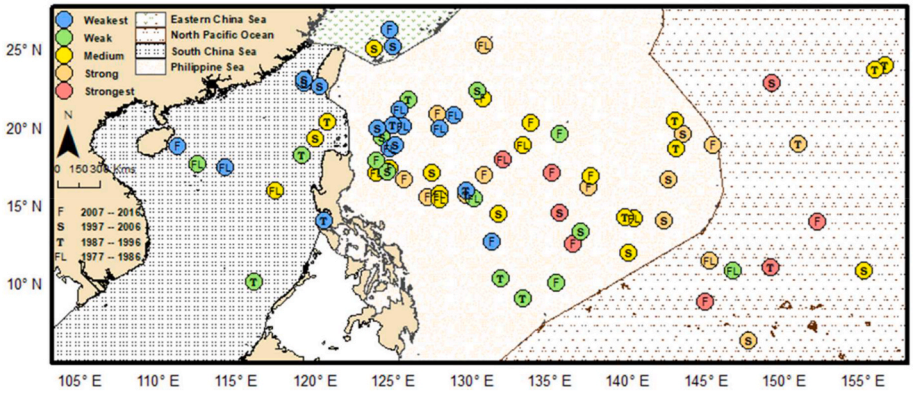


**Fig. 8.** Decadal variation in the strength of typhoons in various oceans for all typhoons that hit Taiwan during 1977–2016. Note that the maximum strength of typhoons is represented by colored dots on cyclogenesis locations. Colors red: strongest (900–920 hPa); orange: strong (921–940 hPa); yellow: medium (941–960 hPa); green: low (961–980 hPa); and blue: weakest (981–998 hPa) typhoon strength class. (For interpretation of the references to color in this figure legend, the reader is referred to the Web version of this article.)

The majority of typhoons (66%) that strike Taiwan originate in the Philippine Sea, which is a marginal sea situated in the East and the Northeast of the Philippines. According to the International Hydrographic Organization, the Philippine Sea is that portion of the North West Pacific (NWP) Ocean, which is off the coasts of the Philippine Islands although, for clarification, the current paper takes both the North Pacific Ocean and the Philippine Sea as two separate identities as shown in the figure below (Fig. 9). 59% of all oceans' originated West directional typhoons to hit Taiwan have cyclogenesis alone in the South China Sea. Also, 83% of the South China Sea originated typhoons that hit

**Table 3**
All typhoon pathways and parameters with their decadal variations classified in their respective oceans of cyclogenesis for typhoons that hit Taiwan during 1977–2016; $n = 77$. Note that D1: 2007–2016, D2: 1997–2006, D3: 1987–1996, and D4: 1977–1986.

| Ocean of cyclogenesis | Frequency (percentage) | Direction | Average Minimum Pressure (in hPa) | Typhoon Pathway over Taiwan | Month of Cyclogenesis | Average Survival (hours) | Average Geodesic track length of typhoon (Kms) | Average Geodesic distance between Cyclogenesis and Cyclolysis locations (Kms) | Average Sinuosity value | Average Sinuosity Index value |
|---|---|---|---|---|---|---|---|---|---|---|
| Philippine Sea | **51 (66%)** (D1: 13; D2: 9; D3: 13; D4: 16) | East (32), South (14), West (5) | **954.9** (D1 ~ D4: 960.7, 964.4, 958.2, 942.2) | 1 (12), 2 (11), 3 (10), 4 (7), 5 (4), 6 (1), 7 (3), 8 (2), 9 (1) | June (5), July (14), Aug (18), Sept (13), Oct (1) | **121.6** (D1 ~ D4: 84.9, 122.7, 117.2, 154.5) | 2192.9 (D1 ~ D4: 1715.2, 2498.0, 1980.5, 2582.1) | 1845.5 (D1 ~ D4: 1425.1, 2117.3, 1795.9, 2074.3) | 1.18 (D1 ~ D4: 1.18, 1.16, 1.11, 1.24) | **4.76** (D1 ~ D4: 4.64, 4.89, 3.80, 5.55) |
| North Pacific Ocean | **11 (14%)** (D1: 2; D2: 4; D3: 3; D4: 2) | East (8), South (2), West (1) | **932.7** (D1 ~ D4: 950, 940, 933.3, 900) | 1 (2), 2 (3), 3 (1), 4 (3), 7 (1), 10 (1) | July (4), Aug (5), Oct (1), Nov (1) | **187.6** (D1 ~ D4: 168, 207, 172, 192) | 3960.9 (D1 ~ D4: 3480.7, 3936.8, 4170.8, 4174.5) | 3504.2 (D1 ~ D4: 3326.0, 3700.7, 3389.1, 3461.9) | 1.13 (D1 ~ D4: 1.05, 1.06, 1.23, 1.20) | **4.61** (D1 ~ D4: 3.59, 3.86, 6.03, 4.97) |
| South China Sea | **12 (16%)** (D1: 3; D2: 4; D3: 4; D4: 1) | West (10), South (2) | **975.8** (D1 ~ D4: 968.3, 970.3, 984.8, 985) | 3 (1), 5 (4), 6 (5), 9 (1), 10 (1) | May (2), June (4), July (3), Aug (1), Sept (2) | **145.5** (D1 ~ D4: 236, 172.5, 67.5, 78) | 2091.8 (D1 ~ D4: 3757.0, 2210.0, 950.0, 1190.8) | 1140.7 (D1 ~ D4: 1660.8, 1123.0, 776.6, 1107.3) | 2.03 (D1 ~ D4: 2.33, 2.56, 1.51, 1.08) | **8.24** (D1 ~ D4: 9.35, 9.38, 7.26, 4.23) |
| Eastern China Sea | **3 (4%)** (D1: 0; D2: 0; D3: 2; D4: 1) | East (1), South (1), West (1) | **979** (D3: 976, D4: 985) | 6 (1), 7 (1), 8 (1) | Aug (1), Sept (2) | **132** (D3: 174, D4: 48) | 1297.1 (D3: 1544.0, D4: 803.3) | 630.9 (D3: 550.0, D4: 792.7) | 1.89 (D3: 2.31, D4:1.01) | **5.75** (D3: 7.44, D4: 2.37) |

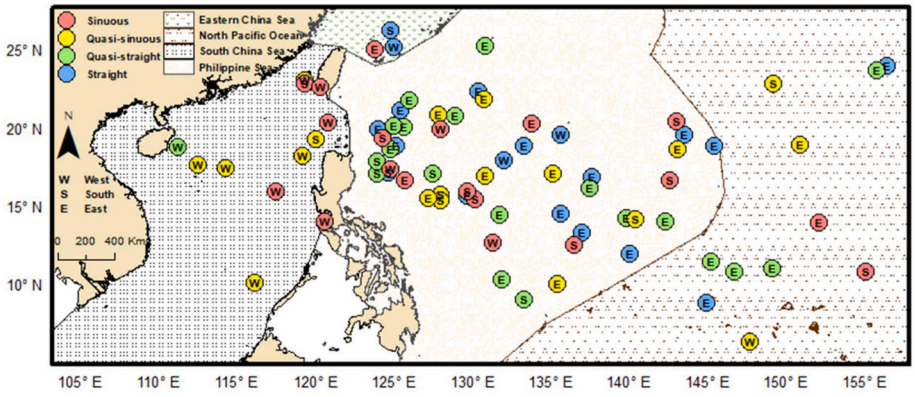


**Fig. 9.** Classification and mapping of ocean of cyclogenesis, track Sinuosity Index (SI) value, and direction of typhoons to hit Taiwan based on cyclogenesis locations on the map for all typhoons during 1977–2016; n = 77. Note here that typhoon track SI values are represented by colored dots on cyclogenesis locations. Colors red: sinuous (SI value > 6.826); yellow: quasi-sinuous (6.826 > SI value > 4.766); green: quasi-straight (4.766 > SI value > 3.165); and blue: straight (3.165 > SI value). (For interpretation of the references to color in this figure legend, the reader is referred to the Web version of this article.)

Taiwan, attacked the country from the West direction. Hence, the South China Sea is the main source of the West striking typhoons to Taiwan. However, the Philippine Sea alone accounts for 78% of all oceans' typhoons and 63% of the only Philippine sea-created typhoons that hit Taiwan from the East direction. Also, 73% of the North Pacific Ocean created typhoons strike Taiwan from the East. The most intense typhoons on average are found in the North Pacific Ocean as the typhoons originated in them get maximum ocean space to gain strength before striking Taiwan in comparison to the other oceans. The analysis of the strength of typhoons based on their cyclogenesis location also supports the above statement, as we see that the most far extended ocean from Taiwan has the lowest average minimum pressure of typhoons and vice-versa. The most intense typhoons are formed over the North Pacific Ocean with an average minimum pressure of 932.7 hPa, which keeps on increasing and reaches 954.9 hPa and 975.8 hPa for the Philippine Sea and the South China Sea, respectively. The least intense typhoons are formed over the Eastern China Sea whose extension is lowest from Taiwan among the four oceans with an average minimum pressure of 979 hPa. Hence, it indicates that the typhoons whose locations of cyclogenesis are close to Taiwan will create less intense typhoons for Taiwan and the intensity of typhoons will keep on increasing as the cyclogenesis location will go far from the land of Taiwan. This statement is also supported by a previous study where the most intense typhoons' cyclogenesis locations were found in most eastern parts of the NWP Ocean with a gradual decrease in typhoons' intensity as we move the western side of the NWP Ocean (Pandey and Liou, 2020a).

As per the literature, it is supposed that the relatively stronger typhoons originated oceans' area will consequently result in more curvy tracks of the typhoons (Terry and Gienko, 2011; Terry et al., 2013; Terry and Kim, 2015). Pandey and Liou (2020a) showed that the most eastern falling cyclogenesis location carrying typhoons have maximum track sinuosity in their paths along with maximum strength in the NWP Ocean basin. This trend keeps on decreasing with the final existence of the minimum track sinuosity typhoons' cyclogenesis location along with the minimum strength at the most western parts of the NWP Ocean basin. If we consider merely the typhoons that hit Taiwan in their life journey, we found that the South China Sea has 79% more track sinuosity than the North Pacific Ocean, even when the South China Sea originated typhoons are 36% on average weaker than those of the North Pacific Ocean originated typhoons. Fig. 9 shows the mapping of three typhoon parameters i.e., ocean of cyclogenesis, typhoon track Sinuosity Index (SI) value, and direction to hit Taiwan based on the cyclogenesis

locations of all typhoons.

The classes of typhoon track SI values are based on dividing all SI values into quartiles by putting an almost equal number of typhoon cases in each quartile. Similar techniques were used in the previous studies to create quartile-based SI classes named, sinuous, quasi-sinuous, quasi-straight, and straight for analyzing typhoon cases in the Atlantic Ocean, the Indian Ocean, the North West Pacific Ocean, and the South Pacific Ocean (Terry and Gienko, 2011; Terry et al., 2013; Terry and Kim, 2015; Pandey and Liou, 2020a). From Fig. 8, it can be perceived very clearly that three-fourths (75%) of all typhoons of the South China Sea belong to the weaker typhoon (961–998 hPa) categories. In contrast, 92% of all typhoons of the South China Sea possess high sinuosity in their tracks belonging to the sinuous track (sinuous and quasi-sinuous: SI value $>$ 4.766) categories. The majority of (90%) typhoons with the sinuous tracks (sinuous and quasi-sinuous: SI value $>$ 4.766) in the South China Sea hit Taiwan from the West direction, while only 11% of the rest of all oceans' typhoons take a Westerly path to attack Taiwan. 74% of the straighter (straight and quasi-straight: SI value $<$ 4.766) path following typhoons strike Taiwan from the East direction only. No sinuous track following typhoon reaches Taiwan from the East. Around 44% of the stronger typhoons only take the Easterly path to enter Taiwan excluding the South China Sea typhoon cases.

These are very crucial findings for the typhoon-prone damages caused to Taiwan. As the sinuosity has a direct association with the damages caused due to the potential failure of accurate movement prediction by the models. The results are alone consistent with the analysis of sub-section 5.2, which reveals that Westerly striking typhoons will on average survive longer with more twists and turns during their path. The South China Sea has a majority of the West striking typhoons. It aids the South China Sea to secure the position of carrying on average the second-longest survival typhoons' (145.5 h) for Taiwan during the study period. This becomes very crucial information for Taiwan's typhoon risk assessment or disaster assessment teams. This information can help them take proper actions by keeping special attention on the typhoons moving from the West of the country, specifically from the South China Sea, due to more errors expected in their predictions.

### 5.5. ENSO phase-wise distribution

The previous studies widely used the Multivariate ENSO Index (MEI) for classifying typhoon events in warm and cold phases by collecting the information about respective months of cyclogenesis of typhoons (Astier et al., 2015; Jien et al., 2015). A recent study utilized the MEI to detect phases of ENSO for typhoons of the NWP Ocean basin and revealed that in the warm ENSO phase the frequency and strength of typhoons rise significantly in the NWP (Pandey and Liou, 2020a). The details about data and methods used for classifying typhoons in ENSO phases using the MEI index are provided in sub-section 4.4. Table 4 provides detailed statistical information about all typhoons classified in terms of their ENSO phases.

Table 4 reveals that the warm phase of ENSO caused around 26% more cyclogenesis than the cold phase of ENSO for all those typhoons of interest in the last 4 decades. There is a distinct and gradual decadal incline in the frequency of typhoons that hit Taiwan in the warm phase of ENSO based on the last 40 years of data. The above pattern indicates that in the future the warm phase of ENSO potentially can produce even more typhoons than the current decade. This is an alarming situation for all typhoon damage handling agencies of Taiwan for prior preparation. In contrast, there is a distinct and gradual decadal decline in the frequency of typhoons that originate during the cold phase of ENSO and hit Taiwan based on the last 4 decades of data. This information is also very crucial to researchers and Taiwan's agencies responsible for disaster management. Fig. 10 shows the comparison of other typhoon parameters with the ENSO phases at the time of cyclogenesis based on mapping on their respective location of cyclogenesis.

Table 4 and Fig. 10 reveal that the cold phase of ENSO creates slightly stronger typhoons on average for Taiwan, but the warm phase of ENSO creates typhoons with slightly more sinuosity in their tracks for Taiwan. Hence, they survive more hours before striking Taiwan. The main reason behind increased track sinuosity of typhoons in the warm phase of ENSO potentially can be (400%) four times more typhoon cases

**Table 4**
All typhoon pathways and parameters with their decadal variations classified in their respective phases of the El Niño Southern Oscillation for typhoons that hit Taiwan during 1977–2016; $n = 77$. Note here that, D1: 2007–2016, D2: 1997–2006, D3: 1987–1996, and D4: 1977–1986.

| ENSO phase | Frequency (percentage) | Typhoon Direction | Typhoon Pathway over Taiwan | Average Minimum Pressure (in hPa) | Ocean of Cyclogenesis | Month of Cyclogenesis | Average Survival (hours) | Average Geodesic track length of typhoon (Kms) | Average Geodesic distance between Cyclogenesis and Cyclolysis locations (Kms) | Average Sinuosity value | Average Sinuosity Index value |
|---|---|---|---|---|---|---|---|---|---|---|---|
| Warm | **29 (38%)** (D1: 9; D2: 9; D3: 8; D4: 3) | East (17), South (5), West (7) | 1 (6), 2 (6), 3 (2), 4 (4), 5 (2), 6 (3), 7 (2), 8 (1), 9 (1), 10 (2) | **956.1** (D1 ~ D4: 955.6, 959.4, 965.1, 923.3) | Philippine Sea (16), North Pacific Ocean (8), South China Sea (5) | June (2), July (8), Aug (12), Sept (5), Oct (1), Nov (1) | **157.4** (D1 ~ D4: 166.7, 162.7, 127.5, 194) | 2843.8 (D1 ~ D4: 3066.9, 2828.6, 2420.9, 3347.8) | 2200.5 (D1 ~ D4: 2069.6, 2287.6, 2110.5, 2571.7) | 1.47 (D1 ~ D4: 1.62 1.67, 1.15, 1.30) | **5.76** (D1 ~ D4: 6.75, 5.49, 4.78, 6.16) |
| Cold | **23 (30%)** (D1: 3; D2: 3; D3: 5; D4: 12) | East (12), South (7), West (4) | 1 (4), 2 (5), 3 (4), 4 (2), 5 (3), 6 (1), 7 (2), 8 (1), 9 (1) | **948.5** (D1 ~ D4: 971.7, 948.3, 970, 933.8) | Philippine Sea (16), South China Sea (4), North Pacific Ocean (2), Eastern China Sea (1) | May (1), June (2), July (8), Aug (5), Sept (6), Oct (1) | **122.9** (D1 ~ D4: 98, 164, 72, 140) | 2198.0 (D1 ~ D4: 1928.8, 3130.0, 1287.5, 2411.7) | 1864.0 (D1 ~ D4: 1525.2, 2474.3, 1194.5, 2075.2) | 1.22 (D1 ~ D4: 1.23, 1.29, 1.31, 1.16) | **5.12** (D1 ~ D4: 5.76, 6.38, 4.67, 4.84) |
| Neutral | **25 (32%)** (D1: 6; D2: 5; D3: 9; D4: 5) | East (12), South (7), West (6) | 1 (4), 2 (3), 3 (6), 4 (4), 5 (3), 6 (3), 7 (1), 8 (1) | **962.7** (D1 ~ D4: 963.3, 968.2, 952.9, 974) | Philippine Sea (19), South China Sea (3), Eastern China Sea (2), North Pacific Ocean (1) | May (1), June (5), July (5), Aug (8), Sept (6) | **120.7** (D1 ~ D4: 59, 133.2, 142, 144) | 2055.1 (D1 ~ D4: 1190.1, 2444.3, 2149.2, 2534.6) | 1662.3 (D1 ~ D4: 1159.8, 2067.8, 1651.6, 1879.1) | 1.27 (D1 ~ D4: 1.03, 1.21, 1.44, 1.30) | **4.98** (D1 ~ D4: 2.93, 5.69, 5.53, 5.77) |

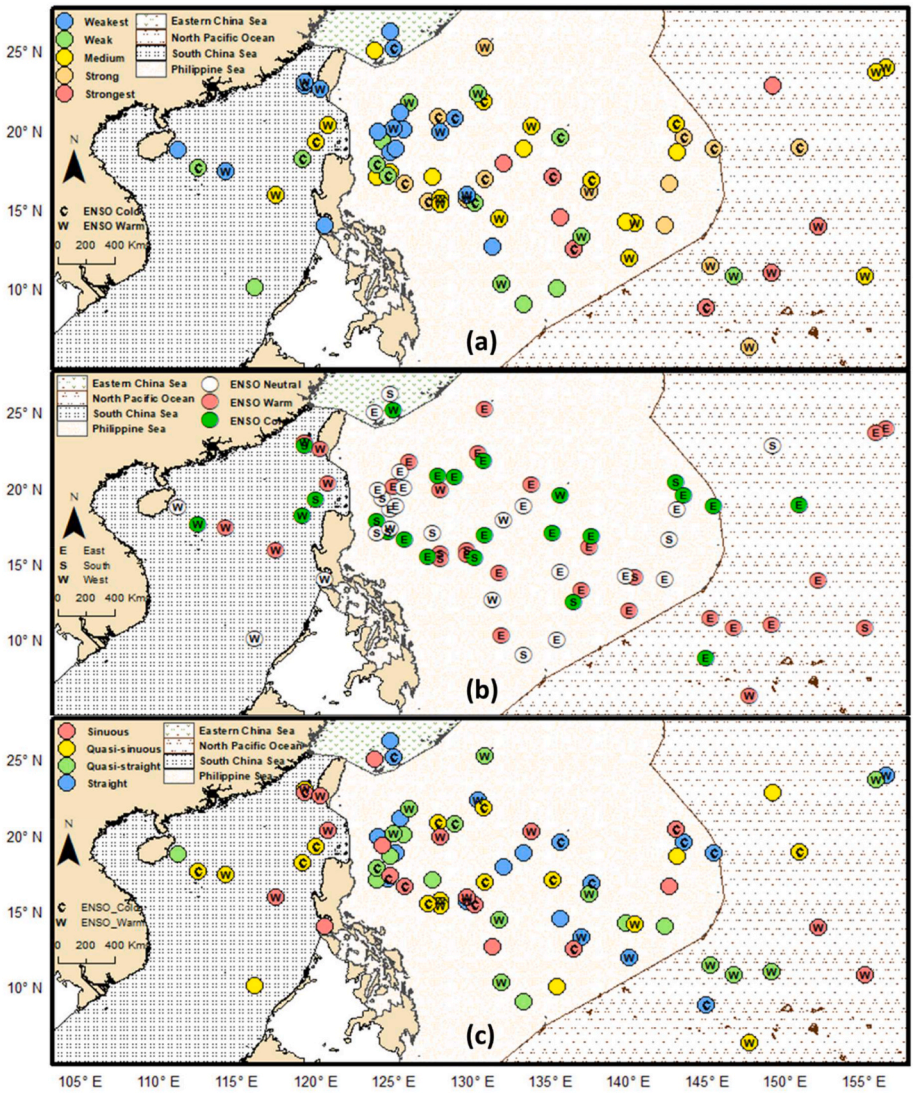


**Fig. 10.** Comparison between phases of the El Niño Southern Oscillation to ocean of cyclogenesis, strength, and direction of typhoons to hit Taiwan based on the cyclogenesis locations on the map for all typhoons that hit Taiwan during the last four decades (1977–2016); n = 77. Note here that for Figure (a); the maximum strength of typhoons is represented by colored dots on cyclogenesis locations. Colors red: strongest (900–920 hPa); orange: strong (921–940 hPa); yellow: medium (941–960 hPa); green: low (961–980 hPa); and blue: weakest (981–998 hPa) typhoon strength class, for the Figure (b); the typhoon's cyclogenesis locations with the warm, cold and neutral phases are represented by red, green and white dots, respectively, and for the Figure (c); the typhoon track SI values are represented by colored dots on cyclogenesis locations. Colors red: sinuous (SI value > 6.826); yellow: quasi-sinuous (6.826 > SI value > 4.766); green: quasi-straight (4.766 > SI value > 3.165); and blue: straight (3.165 > SI value). (For interpretation of the references to color in this figure legend, the reader is referred to the Web version of this article.)

**Table 5**
Frequency of all typhoon's parameters (sinuosity, strength, direction, and ENSO) of typhoons that hit Taiwan during 1977–2016 based on their cyclogenesis locations; ($n = 77$) [a].

| Categories | | Cyclogenesis location latitude | | | | | Cyclogenesis location longitude | | | | |
|---|---|---|---|---|---|---|---|---|---|---|---|
| | | 25–30°N | 20–25°N | 15–20°N | 10–15°N | 05–10°N | 150–160°E | 140–150°E | 130–140°E | 120–130°E | 110–120°E |
| **Sinuosity** | Sinuous | 1 | 5 | 8 | 5 | 0 | 2 | 2 | 4 | 9 | 2 |
| | Quasi–sinuous | 0 | 4 | 11 | 3 | 1 | 1 | 4 | 4 | 4 | 6 |
| | Quasi–straight | 1 | 5 | 6 | 7 | 1 | 1 | 4 | 6 | 8 | 1 |
| | Straight | 2 | 3 | 10 | 3 | 1 | 1 | 3 | 8 | 7 | 0 |
| **Strength** | Strongest, | 0 | 1 | 2 | 4 | 1 | 1 | 3 | 4 | 0 | 0 |
| | Strong | 1 | 1 | 9 | 2 | 1 | 1 | 6 | 3 | 4 | 0 |
| | Medium | 1 | 6 | 10 | 5 | 0 | 3 | 3 | 7 | 7 | 2 |
| | Weak | 0 | 2 | 7 | 5 | 1 | 0 | 1 | 7 | 4 | 3 |
| | Weakest | 2 | 7 | 7 | 2 | 0 | 0 | 0 | 1 | 13 | 4 |
| **Direction** | West | 1 | 3 | 9 | 3 | 1 | 0 | 1 | 3 | 6 | 7 |
| | South | 1 | 3 | 11 | 3 | 1 | 1 | 4 | 3 | 9 | 2 |
| | East | 2 | 11 | 15 | 12 | 1 | 4 | 8 | 16 | 13 | 0 |
| **ENSO** | Warm | 1 | 10 | 7 | 10 | 1 | 4 | 6 | 7 | 9 | 3 |
| | Cold | 1 | 5 | 15 | 1 | 1 | 1 | 4 | 7 | 7 | 4 |
| | Neutral | 2 | 3 | 12 | 7 | 1 | 0 | 4 | 7 | 12 | 2 |

[a] Sinuosity: sinuous (SI value > 6.826), quasi-sinuous (6.826 > SI value > 4.766), quasi-straight (4.766 > SI value > 3.165), and straight (3.165 > SI value). Strength: strongest (900–920 hPa), strong (921–940 hPa), medium (941–960 hPa), low (961–980 hPa), and weakest (981–998 hPa). Direction: according to enter in Taiwan. ENSO: based on month of cyclogenesis of typhoons.

present in the most far North Pacific Ocean in the warm phase than in the cold phase of ENSO. Fig. 10b shows that there is no such significant difference in typhoons' directional patterns between both phases of ENSO.

### 5.6. Statistical analysis

#### 5.6.1. Statistical tests

The divisions of all typhoon-related parameters in various classes as formed in Figs. 7–10, are very essential for better analysis of the cases as well as detection of various hidden patterns. This kind of division of typhoons' various parameters can assist analysis in two ways: (a) by adopting a simplistic mapping approach for understanding through visualization, and (b) by using statistical tests to find out if there is any longitudinal or latitudinal pattern available in various parameters. Moreover, statistical tests can assist for validating the results found in terms of the relationship among all four parameters (sinuosity, strength, direction, and ENSO) under study. In general, creating classes of typhoon parameters facilitates spatial analyses of all parameters under study based on their respective cyclogenesis locations. The current paper uses the Fisher's Exact test of countable data and Two-sided Chi-square ($\chi 2$) tests to check if any statistically significant difference exists both longitude- and latitude-wise in each typhoon-related parameter-class (sinuosity, strength, direction, and ENSO) based on their cyclogenesis position. Detailed comparison and methods of both statistical tests are given in sub-section 4.3. Table 5 shows the frequency of all the above-described typhoon parameters in 5°-latitudinal and 10°-longitudinal zones of all typhoons of interest during 1977–2016.

Pandey and Liou (2020a) used similar 5°-latitudinal and 10°-longitudinal zones to implement the Chi-square ($\chi 2$) test for checking variation between sinuosity index values for the typhoons of the NWP basin. Several previous studies also employed the Chi-square ($\chi 2$) test with 5°-latitudinal and 10°-longitudinal zones to check the variability of typhoon's parameters (Terry and Gienko, 2011; Terry et al., 2013; Terry and Kim, 2015). To apply the statistical tests to Table 5 data, null hypotheses ($H_0$) were created so that no highly significant difference exists in terms of each typhoon-related parameter-classes for cyclogenesis locations between each 10°–longitudinal or 5°–latitudinal zone. Table 6 shows the results of the statistical tests as shown below:

Many combinations of rows have been created for each typhoon-related parameter class to check if any statistically significant variation exists every 5°–latitudinal or 10°–longitudinal zone (Table 6). There is no statistically significant difference existing for the cyclogenesis locations between each 5°–latitudinal zone in the typhoons track sinuosity, intensity, the direction of entering Taiwan, and ENSO phases the typhoons belonging to. Null hypotheses are rejected at $>$ 99.93% confidence level ($p < 0.001$) for the typhoon strength-wise classes in all three-row combinations (with all 5-rows \ 3-rows; strongest + strong, medium, weak + weakest \ 4-rows; strongest + strong, medium, weak, and weakest) by the Fisher's Exact Test for the countable data for cyclogenesis locations between each 10°–longitudinal zone. Although, for the Two-sided chi-square ($\chi 2$) test, the null hypothesis is only rejected once at 99.97% confidence level ($p < 0.001$) for 4-row combination of typhoon strength-wise class for cyclogenesis locations between each 10°–longitudinal zone, several cell values are <5 (less than 5) and 0 (zero) even in some cases. Thus, Two-sided chi-square ($\chi 2$) test-based results are not so reliable over Fisher's Exact Test for countable data. Consequently, a statistically significant difference exists between each 10°–longitudinal zone in typhoons' strength based on the place of cyclogenesis.

The above result is entirely in a sink with the preceding analysis in this paper (sub-section 5.4) on the variation of typhoons' strength based on the ocean of cyclogenesis. It was shown that the distribution of most intense typhoons based on the cyclogenesis location is over the most far extended oceans from the land of Taiwan and vice-versa. Hence, the North Pacific Ocean possesses on average the maximum intense

**Table 6**
Results of Fisher's Exact and Two-sided chi-square ($\chi 2$) tests for all parameters (sinuosity, strength, direction, and ENSO phases) of typhoons of interest during 1977–2016 based on their cyclogenesis locations; ($n = 77$).

| Categories | Results latitude-wise | Null ($H_0$) hypothesis | Results longitude-wise | Null ($H_0$) hypothesis |
|---|---|---|---|---|
| **Sinuosity** | (1) Fisher's Exact Test: p = 0.801<br>(2) Two-sided chi-square ($\chi 2$): p = 0.807 | **selected**<br>**selected** | (1) Fisher's Exact Test: p = 0.320<br>(2) Two-sided chi-square ($\chi 2$): p = 0.254 | **selected**<br>**selected** |
| **Strength** | (1) Fisher's Exact Test: p = 0.272 (with 5 rows)<br>(2) Fisher's Exact Test: p = 0.762 (with 3 rows; strongest + strong, medium, weak + weakest)<br>(3) Fisher's Exact Test: p = 0.414 (with 4 rows; strongest + strong, medium, weak, weakest)<br>(4) Two-sided chi-square ($\chi 2$): p = 0.333 (with 5 rows)<br>(5) Two-sided chi-square ($\chi 2$): p = 0.729 (with 3 rows; strongest + strong, medium, weak + weakest)<br>(6) Two-sided chi-square ($\chi 2$): p = 0.414, (with 4 rows; strongest + strong, medium, weak, weakest) | **selected**<br>**selected**<br>-<br>**selected**<br>-<br>**selected**<br>**selected**<br>-<br>**selected** | (1) Fisher's Exact Test: p = 2.2E-04 and $p < 0.001$ (with 5 rows)<br>(2) Fisher's Exact Test: p = 6.5E-04 and $p < 0.001$ (with 3 rows; strongest + strong, medium, weak + weakest)<br>(3) Fisher's Exact Test: p = 1.7E-04 and $p < 0.001$ (with 4 rows; strongest + strong, medium, weak, weakest)<br>(4) Two-sided chi-square ($\chi 2$): p = 0.0015 (with 5 rows)<br>(5) Two-sided chi-square ($\chi 2$): p = 0.0014 (with 3 rows; strongest + strong, medium, weak + weakest)<br>(6) Two-sided chi-square ($\chi 2$): p = 0.0004 and $p < 0.001$ (with 4 rows; strongest + strong, medium, weak, weakest) | **rejected**<br>**rejected**<br>-<br>**rejected**<br>-<br>**selected**<br>**selected**<br>-<br>**rejected** |
| **Direction** | (1) Fisher's Exact Test: p = 0.763 (with 3 rows)<br>(2) Fisher's Exact Test: p = 0.625 (with 2 rows; east, west)<br>(3) Two-sided chi-square ($\chi 2$): p = 0.829 (with 3 rows) | **selected**<br>**selected**<br>**selected**<br>**selected** | (1) Fisher's Exact Test: p = 0.002 (with 3 rows)<br>(2) Fisher's Exact Test: p = 2.8E-04 and $p < 0.001$ (with 2 rows; east, west)<br>(3) Two-sided chi-square ($\chi 2$): p = | **selected**<br>**rejected**<br>-<br>**selected**<br>**rejected** |

(continued on next page)

**Table 6** (*continued*)

| Categories | Results latitude-wise | Null ($H_0$) hypothesis | Results longitude-wise | Null ($H_0$) hypothesis |
|---|---|---|---|---|
| | (4) Two-sided chi-square ($\chi 2$): p = 0.688 (with 2 rows; east, west) | | 0.0015 (with 3 rows)<br>(4) Two-sided chi-square ($\chi 2$): p = 0.0002 and p < 0.001 (with 2 rows; east, west) | |
| **ENSO** | (1) Fisher's Exact Test: p = 0.026 (with 3 rows)<br>(2) Fisher's Exact Test: p = 0.007 (with 2 rows; warm, cold)<br>(3) Two-sided chi-square ($\chi 2$): p = 0.085 (with 3 rows)<br>(4) Two-sided chi-square ($\chi 2$): p = 0.022 (with 2 rows; warm, cold) | **selected**<br>**selected**<br>**selected**<br>**selected** | (1) Fisher's Exact Test: p = 0.644 (with 3 rows)<br>(2) Fisher's Exact Test: p = 0.781 (with 2 rows; warm, cold)<br>(3) Two-sided chi-square ($\chi 2$): p = 0.549 (with 3 rows)<br>(4) Two-sided chi-square ($\chi 2$): p = 0.735 (with 2 rows; warm, cold) | **selected**<br>**selected**<br>**selected**<br>**selected** |

typhoons with an average minimum pressure of 932.7 hPa, which increases as we move close to Taiwan with an average minimum pressure of 954.9 hPa, 975.8 hPa, and 979 hPa for the Philippine Sea, the South China sea, and the Eastern China Sea, respectively. Thus, the statistical Fisher's Exact test for countable data verifies the preceding results in this case. Null hypotheses are rejected by both Fisher's Exact test for countable data and the Two-sided chi-square ($\chi 2$) test for cyclogenesis locations between each 10°–longitudinal zone at 99.97% confidence level ($p < 0.001$) for the typhoon direction-wise class with two-row combinations of the East and the West striking direction of typhoons to Taiwan. Hence, there is a statistically significant longitudinal variation in the cyclogenesis locations of typhoons that hit Taiwan from the East or the West direction. The results are similar to the previous analysis in this paper (sub-section 5.2) where the majority of cyclogenesis locations of the West striking typhoons to Taiwan lie in the most West ocean like the South China Sea with around 59% of such typhoons. Nevertheless, 78% of all typhoons that strike Taiwan from the East alone have cyclogenesis in the Philippine Sea. Also, around 73% of typhoons whose cyclogenesis is in the North Pacific Ocean hit Taiwan from the East direction. Hence, the statistical tests verify the earlier results in this case.

Although both statistical tests select the null hypothesis showing that there is no significant variation in typhoons' track sinuous nature longitude-wise based on the place of cyclogenesis, which is just opposite of the earlier studies that found typhoons' track sinuosity directly proportional to typhoons' intensity (Terry and Gienko, 2011; Terry et al., 2013; Terry and Kim, 2015; Pandey and Liou, 2020a). However, the above statistical tests' results are fully verifying the results observed in this paper earlier in sub-section 5.2, showing that 75% of all typhoons of the South China Sea are weaker typhoons (961–998 hPa) though 92% of all typhoons of the South China Sea possess the high sinuous nature of tracks of typhoons (SI value > 4.766). In contrast, typhoons of the North Pacific Ocean have the highest average typhoons' intensity (932.7 hPa), but almost half track Sinuosity Index values (SI = 4.61) in comparison to the South China Sea (SI = 8.24). Thus, the statistical tests are wholly in the sink with the analysis done in this case in this paper. There are no significant longitudinal variations in cyclogenesis places based on the ENSO phases, which are again consistent with the ENSO analysis results in this paper, despite the fact that 26% of more typhoons originate during the warm ENSO phase than in the cold ENSO phase. Note that the previous study also has shown more than a double-increase in the number of typhoons in the warm ENSO phase than the cold ENSO phase considering the cases for the whole North West Pacific (Pandey and Liou, 2020a). Despite the similarity, the previous study had shown more accumulation of typhoons in the Eastern part of the NWP during the warm phase of ENSO, which is not the case if we consider only typhoons that strike Taiwan in their life journey.

In summary, statistical tests are very crucial to verify the results along with aiding for better analysis. Results of the statistical tests from Table 6 are solely consistent with all the results in this paper and hence validate them.

### 5.6.2. *Relationship between typhoon parameters*

Fig. 11 shows the relationship among various typhoon parameters under study in the current paper.

Table 7 shows various statistical correlations between parameters of all typhoons of interest in the last 40 (1977–2016) years.

Fig. 11f tells the obvious fact if a typhoon stays longer, it has great potential to cover longer distances as well (r = 0.83). We calculated the correlation between typhoon track SI and typhoon duration and found that the correlation is 0.67, which is greater than the previously measured correlation between the same parameters over the NWP basin during the same period (r = 0.55) (Table 7, Fig. 11a), while the correlation between typhoon track SI and duration for the typhoons of interest during 1977–2016 is 0.42, which is similar (r = 0.48) to the earlier calculated correlation between same parameters over the NWP basin during the same 40 years (Table 7, Fig. 11b). In contrast, the correlation between typhoon track SI and the minimum pressure of all 77 typhoons that strike Taiwan during 1977–2016 is −0.02, whereas the previous study shows the correlation between the same parameters under the same time frame for all 959 typhoons of the NWP basin is −0.35 (Table 7, Fig. 11c) (Pandey and Liou, 2020a).

It is a very significant finding if the typhoons of interest possess more twists and turns, they can survive longer, but not necessarily to be strong in their nature. The above finding is supported by many previous section results showing that the South China Sea has the maximum average SI values (8.24), but on average with the weakest typhoons (975.8 hPa). The correlations between typhoons' minimum pressure and duration or distance covered are negative (r = −0.45 and −0.51, respectively) and not very strong like the correlation between typhoon track SI and duration (Fig, 11a, 11d, 11e). It tells that the strong typhoons of interest have moderate potential to cover longer distances and survive longer hours. Although, on average, most strong typhoons (932.7 hPa) come to Taiwan from the North Pacific Ocean covering the maximum distance (3960.9 km) and surviving the longest hours (187.6 h), but less in frequency than the typhoons coming from the Philippine and the South China Seas. Also, the South China Sea originated typhoons cover on average less distance (1140.7 km), although on average they survive (145.5 h) longer than those of the Philippine Sea due to the highest track sinuosity of this ocean. Hence, it is found that typhoons' track sinuosity plays a more crucial role in the longer survival of typhoons than its strength for the case of typhoons that strike Taiwan.

## 5.7. *Climatological analysis*

A climatological analysis is very crucial to understand the physical reasons behind the various patterns observed in the nature of tracks of typhoons that hit Taiwan in the last 40 years (1977–2016) (James et al., 2006). 10-yearly (Decadal), 5-yearly, yearly, ENSO phase-wise, and month-wise climatological analyses for the whole typhoon season (May–November) over the entire global ocean, the North Pacific Ocean, the Philippine Sea, the South China sea, and the Eastern China Sea are

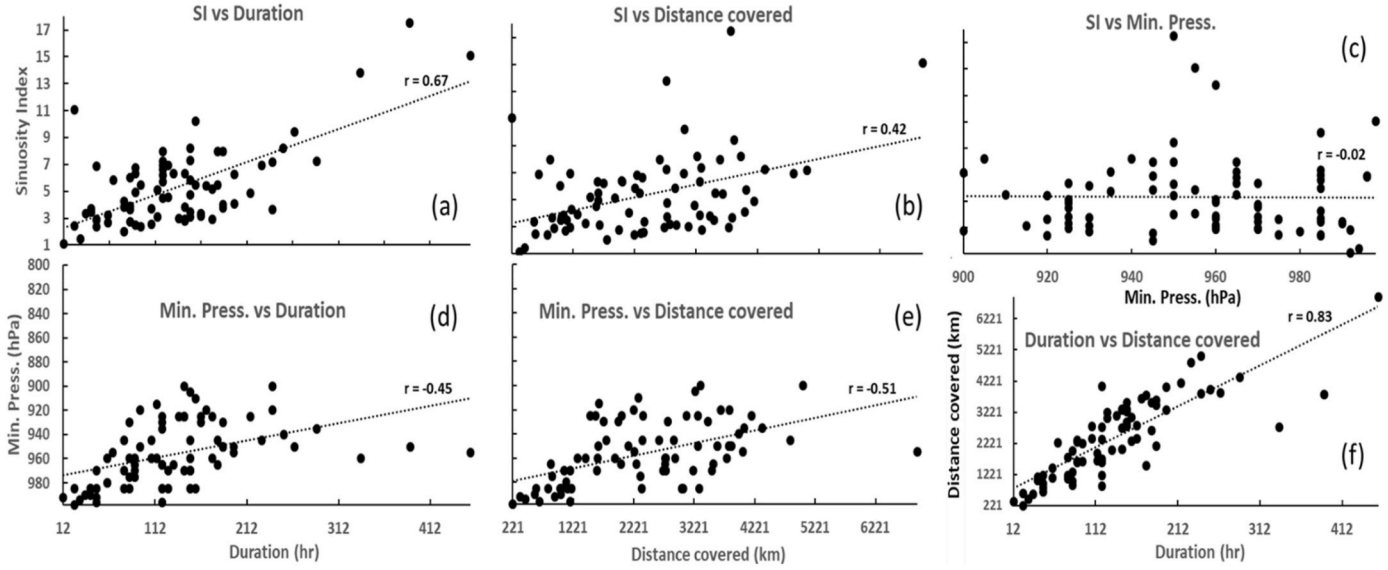


**Fig. 11.** Relationship between (a) sinuosity index and duration (hr), (b) sinuosity index and distance covered (km), (c) sinuosity index and minimum pressure (hPa), (d) minimum pressure (hPa), and duration (hr), (e) minimum pressure (hPa) and distance covered (km), and (f) duration (hr) and distance covered (km) of all typhoons that hit Taiwan during 1977–2016.

**Table 7**
Pearson's correlation between all typhoons' (a) track SI and duration, (b) track SI and distance covered, and (c) track SI and minimum pressure, (d) minimum pressure and duration, (e) minimum pressure and distance covered, and (f) duration and distance covered (n = 77) over 1977–2016.

| Parameters for Correlation | Correlation coefficient (r) | Level of significance (by *t*-test) (*p*) |
|---|---|---|
| SI and Duration (hr) | 0.67 | <0.001 |
| SI and Distance covered (km) | 0.42 | <0.001 |
| SI and Minimum pressure (hPa) | −0.02 | <0.001 |
| Minimum pressure (hPa) and Duration (hr) | −0.45 | <0.001 |
| Minimum pressure (hPa) and Distance covered (km) | −0.51 | <0.001 |
| Duration (hr) and Distance covered (km) | 0.83 | <0.001 |

done throughout 1977–2016 by quantifying the Sea Surface Temperature Anomaly (SSTA) (°C) using the base years 1941–1970. Please refer to sub-sections 4.1 and 4.5 for details about the data used and the methods involved.

*5.7.1. 5-yearly SSTA analysis*

Fig. 12 shows the Sea Surface Temperature Anomaly (SSTA) (°C) averaged 5-yearly over typhoon season for each preceding 5-year period from 1977 to 2016 as well as for the whole study period. The base years are 1941–1970 (30-years). Please refer to sub-section 4.5 for details about the methodology for the 5-yearly SSTA calculations.

Based on the above maps of Fig. 12, Table 8 shows the values of SSTA clearly distributed for all study oceans along with the entire ocean portion of the earth i.e., the global ocean. Fig. 12 and Table 8 effectively indicate the gradual increase of 5-yearly averaged Sea Surface Temperature globally and over the study oceans during the study period (1977–2016) for the whole typhoon season (May–November). From 1977 to 1981 to 2012–2016, the positive anomaly has increased to 250.8% (1.20–4.21 °C), while the negative anomaly has decreased to 44.4% (−0.99 ~ −1.43).

More recent 5-years 2012–2016 have shown an increase of 0.4 °C SSTA globally in comparison to 1977–1981, while in the same period SSTA has increased maximum in the North Pacific Ocean among all study oceans with 0.69 °C, and 0.65 °C, 0.63 °C, and 0.53 °C, respectively, in the Eastern China Sea, the South China Sea, and the Philippine Sea. In comparison to base years (1941–1970), the most recent 5-year (2012–2016) SSTA has increased to 0.44 °C globally, while in the same period SSTA has increased maximum in the Eastern China Sea among all study oceans with 0.72 °C, and 0.71 °C, 0.64 °C, and 0.58 °C, respectively, in the South China Sea, the Philippine Sea, and the North Pacific Ocean. A similar recent study using the 6-yearly (2001–2005) SSTA analysis over the Western Pacific with the paleo-climate data showed that the oceans are getting warmer than the base years of 1951–1980 (James et al., 2006). However, another recent study showed that this increasing SST in the NWP is associated with the increasing strength of typhoons in the region (Mei et al., 2015).

Hence, it is clear that the SSTA has a range of change between 0.4 and 0.7 °C, whether it is compared between the last 4 decades or from 30-years of the base period based on 5-yearly, averaged SSTA data for the typhoon season (May–November). The global ocean has consistently shown the lowest change of SSTA in comparison to all four oceans under study.

*5.7.2. Decadal SSTA analysis*

Fig. 13 shows the decadal Sea Surface Temperature Anomaly (SSTA) (°C) averaged over the typhoon season for each preceding 10-year period from 1977 to 2016. The base years are from 1941 to 1970 (30-years). Please refer to sub-section 4.5 for details about the methodology for decadal SSTA calculations.

Based on the above maps of Fig. 13, Table 9 shows the values of SSTA clearly distributed for all study oceans along with the global ocean. Note that Fig. 12i belongs to SSTA values for all study oceans, but is given in Table 8 to reduce space for Table 7.

Fig. 13 and Table 9 effectively indicate the gradual increase of decadal averaged Sea Surface Temperature globally and over the study area during the study period (1977–2016) for the whole typhoon season (May–November). From 1977 to 1986 to 2007–2016, the positive anomaly has increased to 266.9% (1.12–4.11 °C), while the negative anomaly has decreased to 8.7% (−1.38 ~ −1.50). The most recent decade 2007–2016 has shown an increase of 0.3 °C SSTA globally in comparison to 1977–1986, while, in the same period, the SSTA has increased maximum in the Eastern China Sea among all study oceans by 0.51 °C, and 0.44 °C, 0.44 °C, and 0.41 °C, respectively, in the Philippine Sea, the South China Sea, and the North Pacific Ocean. In comparison to

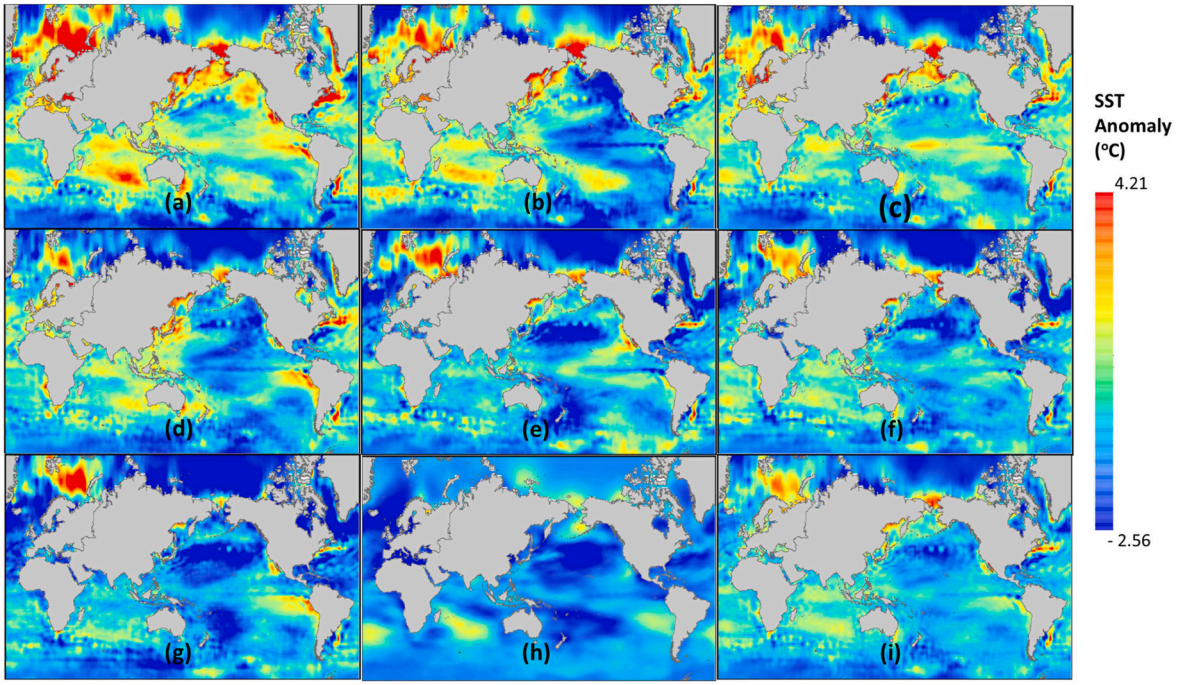


**Fig. 12.** Sea Surface Temperature Anomaly (SSTA) (°C) for the typhoon season (May–November) over the entire global ocean using the base years 1941–1970 and averaged 5-yearly over periods (a) 2012–2016, (b) 2007–2011, (c) 2002–2006, (d) 1997–20 012, (e) 1992–1996, (f) 1987–1991, (g) 1982–1988, and (h) 1977–1981, and averaged 40-yearly over the entire study period of (i) 1977–2016. The maximum (4.21 °C) and minimum (−2.56 °C) SSTA values on colorbar are adopted from the biggest maximum and lowest minimum SSTA values recorded among all, which belong from (a) 2012–2016 (maximum SSTA) and (g) 1982–1986 (minimum SSTA), respectively.

the 30 years base period (1941–1970), the most recent decade 2007–2016 has shown an increase of 0.37 °C SSTA globally, i.e., for the global ocean, while, in the same time period, the SSTA has increased maximum in the Eastern China Sea among all study seas with 0.65 °C, and 0.58 °C, 0.57 °C, and 0.36 °C, respectively, in the Philippine Sea, the South China Sea, and the North Pacific Ocean. Hence, it is clear that the SSTA decadal change has a range of around 0.3–0.5 °C when it is compared between the last 4 decades and around 0.4–0.7 °C compared to the 30-year base period for the typhoon season (May–November). The global ocean has consistently shown a lower change of SSTA in comparison to all oceans under study. The Pacific Ocean alone accounts for almost 80% of typhoons that reach Taiwan, which can be linked to the fact that the Philippine Sea has the second biggest positive change in SSTA in the recent decade during the typhoon season months from May to November. Nevertheless, the maximum variation in SSTA in the recent decade in the Eastern China Sea is potentially due to its closeness to lands, resulting from the first time recorded typhoons in this ocean starting from the last two decades.

Overall, the decadal gradual increase in SST is the potential cause of the decadal-wise increasing strength of typhoons in the region, especially in Taiwan. This is resulting in almost half (50%) of the strongest (900–920 hPa) and 43% of strong (921–940 hPa) typhoons that hit Taiwan from the current decade (F: 2007–2016). In contrast, half (50%) of the typhoons in the fourth decade (FL: 1977–1986) and 47% of typhoons from the third decade (T: 1987–1996) have weak intensity (961–998 hPa), in comparison to only 30% of typhoons with weak intensity from the current decade (2007–2016). As more than half (53%) of the total typhoons to Taiwan hit the country from the East only so that the overall impact on these typhoons' strength is more than the other direction typhoons to Taiwan in the region. Hence, the decadal climatological investigations totally support the decadal intensifications in the strength of typhoons in the study region. A recent study also tells that the decadally growing strength of typhoons in the NWP is a combined effect of changes in SST and vertical wind shear (Zhao et al., 2014).

### 5.7.3. *Yearly SSTA analysis*

Fig. 14 shows the yearly-wise SSTA averaged over the whole typhoon season (May–November) from 1977 to 2016 for all study oceans. The base years are 1941–1970 (30 years). Please refer to sub-section 4.5 for details about the methodology for yearly SSTA measurements.

The yearly climatological investigation is done by measuring SSTA for typhoon season over study oceans and the global ocean using Fig. 14, which shows an overall gradually increasing trend of SSTA in all oceans during the study years (1977–2016). These results are completely in the sink with the previous decadal and 5-yearly SSTA investigations, indicating that the Eastern China Sea has topped with maximum SSTA values, while the lowest SSTA values are in the North Pacific Ocean and almost equal for the Philippine Sea and the South China Sea. In case of a continuous linear trend, we can expect the SSTA change may reach around 1 °C in the next decade for the Eastern China Sea, while 0.5 °C for the North Pacific Ocean and global ocean (Fig. 14a). Similarly, the SSTA change may reach 0.9 °C for the Philippine and South China Seas in the next 10 years (up to 2026).

The major El-Niño epochs during the study years were 1982–83, 1997–98, and 2015–16, which are reflected by the peak positive SSTA values in the Eastern China Sea (1st in 1998, 2nd in 2016), the Philippine Sea (1st in 1998, 2nd in 2016), the South China Sea (1st in 1998, 2nd in 2016), the North Pacific Ocean (1st in 2015, 2nd in 2016), and global ocean (1st in 2016, 2nd in 2015). However, the major La-Niña epochs during the study years were 1988–89, 1998–2000, 2007–08, 2010–11, which are not reflected by the lowest SSTA values in the Eastern China Sea (1st in 1979, 2nd in 1992), the Philippine Sea (1979), the South China Sea (1st in 1984, 2nd in 1985), the North Pacific Ocean (1987), and global ocean (1978). Here, the major El Niño and La Niña epochs are based on the Oceanic Niño Index (ONI) and adopted from the online site of NOAA (https://ggweather.com/enso/oni.htm). A recent study shows that the El Niño cycles influence tropical cyclone activities and rainfall across the Korean Peninsula (Kim et al., 2015). Hence, the role of El-Niño epochs is found very crucial for the SSTA changes during

**Table 8**
5-year Sea Surface Temperature Anomalies of all study oceans over 1977–2016. Mx, Mn, and MN: maximum, minimum, and mean SSTA (°C).

5-yearly Averaged Sea Surface Temperature (°C) Anomaly during whole typhoon Season (May–November); Base period: 1941–1970

| Time Period | 2012–2016 | | | 2007–2011 | | | 2002–2006 | | | 2001–1997 | | | 1992–1996 | | | 1987–1991 | | | 1982–1986 | | | 1977–1981 | | |
|---|---|---|---|---|---|---|---|---|---|---|---|---|---|---|---|---|---|---|---|---|---|---|---|---|
| **Ocean of Cyclogenesis** | Mx | Mn | MN | Mx | Mn | MN | Mx | Mn | MN | Mx | Mn | MN | Mx | Mn | MN | Mx | Mn | MN | Mx | Mn | MN | Mx | Mn | MN |
| Eastern China Sea | 1.44 | 0.09 | 0.72 | 1.34 | −0.29 | 0.57 | 1.51 | 0.04 | 0.68 | 1.68 | 0.19 | 0.83 | 0.94 | −0.17 | 0.33 | 0.86 | −0.38 | 0.23 | 0.70 | −0.21 | 0.20 | 0.25 | −0.30 | 0.07 |
| Philippine Sea | 0.93 | −0.12 | 0.64 | 0.86 | −0.04 | 0.52 | 0.91 | 0.03 | 0.49 | 1.10 | 0.37 | 0.68 | 0.71 | −0.44 | 0.30 | 0.75 | −0.23 | 0.34 | 0.55 | −0.42 | 0.17 | 0.31 | −0.13 | 0.11 |
| South China Sea | 1.28 | 0.38 | 0.71 | 0.98 | −0.05 | 0.44 | 1.21 | 0.20 | 0.52 | 1.21 | 0.35 | 0.69 | 1.10 | −0.09 | 0.33 | 1.02 | 0.01 | 0.43 | 0.71 | −0.21 | 0.18 | 0.23 | −0.10 | 0.08 |
| North Pacific Ocean | 2.77 | −0.37 | 0.58 | 1.73 | −0.94 | 0.14 | 2.02 | −0.58 | 0.34 | 2.19 | −0.72 | 0.17 | 2.25 | −1.20 | 0.16 | 1.91 | −1.02 | 0.13 | 2.02 | −1.26 | 0.01 | 0.56 | −0.99 | −0.11 |
| **Glonal Ocean** | 4.21 | −1.43 | 0.44 | 4.05 | −1.57 | 0.29 | 3.74 | −1.77 | 0.33 | 3.85 | −1.27 | 0.27 | 3.52 | −2.03 | 0.16 | 3.49 | −2.40 | 0.19 | 2.21 | −2.56 | 0.09 | 1.20 | −0.99 | 0.04 |

typhoon season as it influences the SST resulting in more cyclogenesis.

Interestingly, it is found that in all decadal, 5-yearly, and yearly SSTA measurements during the last 40 years, the North Pacific Ocean's SSTA values are closer to the global ocean than any other ocean under study. The cause behind this is obvious, as geographically speaking the North Pacific Ocean is the second biggest ocean after the global ocean among all oceans under study. In fact, it is several times bigger in area than the Philippine Sea, the South China Sea, and the Eastern China Sea (Fig. 1). It is extended roughly between 130° E and 180° E longitude and between the equator and 55° N latitude. Thus, due to the huge size of the North Pacific Ocean, the sea surface temperature over the area is averaged and reaches closer to the global ocean than other oceans under study. Moreover, small oceans can potentially save their peculiarity than bigger oceans.

Following the above, it is also found that in all decadal, 5-yearly, and yearly SSTA measurements during the last 40 years, the Eastern China Sea has shown the maximum SST change. It is potentially due to a combination of several factors as (a) it is surrounded by lands and islands of China and Japan, where SST values close to coasts have been rapidly recorded increasing in the recent few decades due to the effect of global warming (Figs. 12–14, and (b) its overall size is small in comparison to the other study oceans (Fig. 1). Despite discussing the above, a further investigation in the future can be crucial to clarify the cause.

The need of measuring all decadal, 5-yearly, and yearly SSTA patterns together in the study oceans was provided in this paper because of two major reasons addressed as follows: (a) it provides a very clear idea when SST variations were smaller for a longer period of time, for which decadal SST measurements were enough, and when SST variations are so quick in a quite small period of time, especially in the recent decades due to global warming, that we even need yearly SST measurements for analysis properly, and (b) the yearly changing factors like El Niño and La-Niña years need yearly SSTA whereas directional, strength and curviness based factors are easier to compare with half-decadal or decadal SSTA.

### *5.7.4. ENSO phase-wise SSTA analysis*

Fig. 15 shows the ENSO phase-wise SSTA variations in all study oceans. Details of ENSO phase-wise SSTA analysis methodology are explained in sub-section 4.5.

Fig. 15 shows that the SSTA gradually increasing in both ENSO phases in the last 4 decades in most of the study oceans with an exception of maximum SSTA of the Eastern China Sea and the South China Sea during 1997–2006 in ENSO warm and cold phases, respectively. In the majority, the SSTA changes in every decade in all oceans are more during ENSO cold phase. The SSTA values have reached up to 1.01 °C, 0.79 °C, 0.69 °C, 0.32 °C, 0.40 °C, and 0.21 °C, 0.56 °C, 0.81 °C, 0.85 °C, 0.52 °C for the ENSO cold and warm phases in the Eastern China Sea, the Philippine Sea, the South China Sea, the North Pacific Ocean, and global ocean, respectively. Decade-wise gradually increasing SSTA during ENSO phases is consistent with the overall increase of the strength of typhoons that hit Taiwan and also with the previous studies showing the increasing intensity of typhoons in the whole NWP region (Pandey et al., 2021).

### *5.7.5. Monthly SSTA analysis*

Fig. 16 shows monthly (from May to November) variations in SSTA for the study oceans during 1977–2016. Details of the methodology are provided in sub-section 4.5.

It is clear that maximum SSTA change has occurred in the month of May in the Eastern China Ocean. The SSTA has decade-wise gradually increased for continuous three decades (199–2007) in all months of typhoons in all oceans except the Eastern China Sea. The Eastern China Sea has an alternating decadal variation pattern of SSTA in the month of May, making forth (1977–1986) and second decade (1997–2006) SSTA more than the first (2007–2016) and third decade (1987–1996). It is a very interesting outcome and needs further detailed investigations. Both

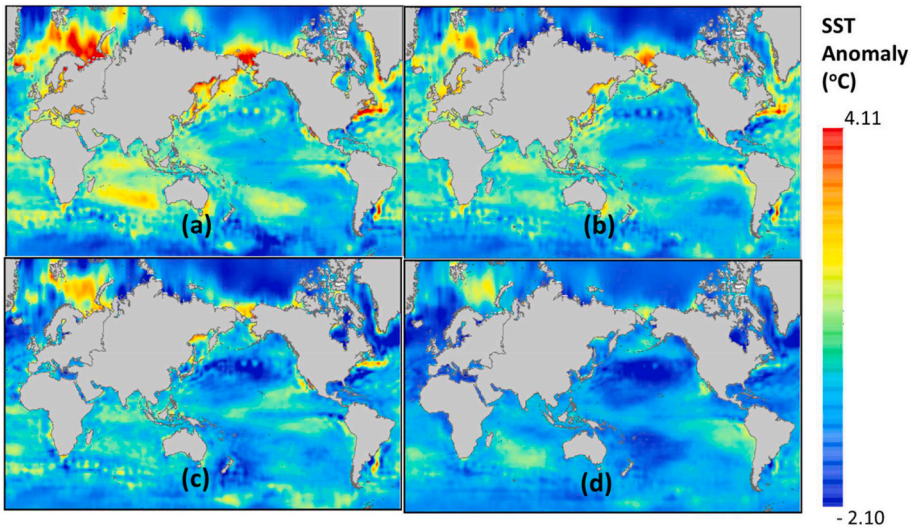


**Fig. 13.** Sea Surface Temperature Anomaly (SSTA) (°C) for the typhoons season (May–November) over the entire global ocean using the base years 1941–1970 and averaged 10-yearly over periods (a) 2007–2016, (b) 1997–2006, (c) 1987–1996, and (d) 1977–1986. The maximum (4.11 °C) and minimum (−2.10 °C) SSTA values on colorbar are adopted from the biggest maximum and lowest minimum SSTA values recorded among all decades, which belong from (a) 2007–2016 (maximum SSTA) and (g) 1987–1996 (minimum SSTA), respectively.

**Table 9**
Decadal and whole study period (1977–2016) averaged Sea Surface Temperature Anomalies of all study oceans. Mx, Mn, and MN: maximum, minimum, and mean SSTA (°C), respectively.

| Decadal Averaged Sea Surface Temperature (°C) Anomaly during whole typhoon Season (May–November); Base period: 1941–1970 | | | | | | | | | | | | | | | |
|---|---|---|---|---|---|---|---|---|---|---|---|---|---|---|---|
| Time Period | 2007–2016 | | | 1997–2006 | | | 1987–1996 | | | 1977–1986 | | | 1977–2016 | | |
| **Ocean of Cyclogenesis** | Mx | Mn | MN | Mx | Mn | MN | Mx | Mn | MN | Mx | Mn | MN | **Mx** | **Mn** | **MN** |
| Eastern China Sea | 1.39 | −0.10 | 0.65 | 1.59 | 0.12 | 0.77 | 0.81 | −0.22 | 0.28 | 0.40 | −0.16 | 0.14 | **0.96** | **−0.05** | **0.46** |
| Philippine Sea | 0.84 | −0.08 | 0.58 | 1.00 | 0.22 | 0.58 | 0.64 | −0.29 | 0.32 | 0.36 | −0.26 | 0.14 | **0.66** | **−0.03** | **0.41** |
| South China Sea | 1.13 | 0.22 | 0.57 | 1.19 | 0.28 | 0.60 | 1.06 | −0.04 | 0.38 | 0.42 | −0.07 | 0.13 | **0.95** | **0.11** | **0.42** |
| North Pacific Ocean | 2.25 | −0.30 | 0.36 | 2.10 | −0.53 | 0.29 | 2.08 | −0.94 | 0.15 | 1.07 | −0.95 | −0.05 | **1.87** | **−0.61** | **0.18** |
| **Global Ocean** | 4.11 | −1.50 | 0.37 | 3.80 | −1.30 | 0.30 | 3.51 | −2.10 | 0.18 | 1.12 | −1.38 | 0.07 | 3.05 | −1.38 | 0.23 |

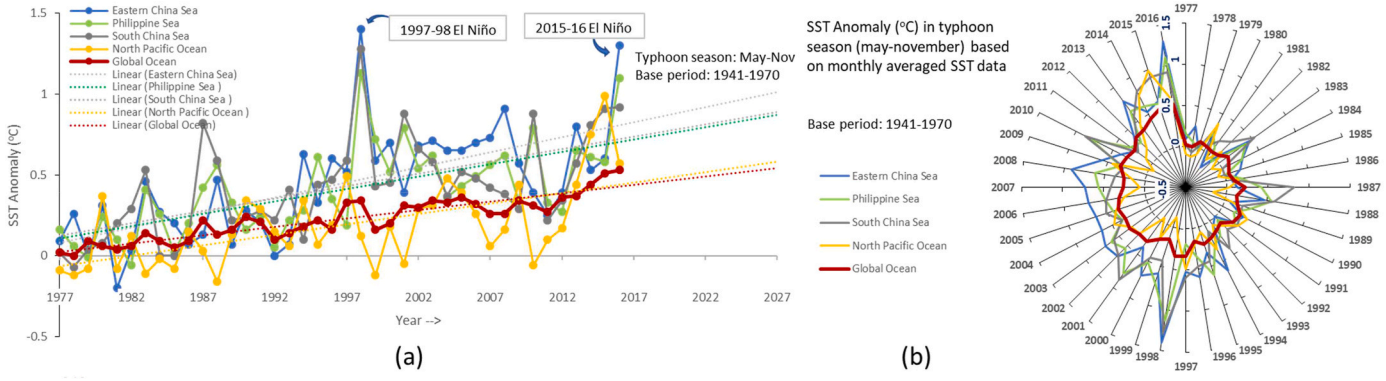


**Fig. 14.** Sea Surface Temperature Anomaly (SSTA) (°C) for the whole typhoon season (May–November) for each year over the entire global ocean, Eastern China Sea, Philippine Sea, South China Sea, and North Pacific Ocean during 1977–2016 using the base years 1941–1970.

the North Pacific Ocean and the global ocean have possessed a continuous decadal increase in SSTA in all months, which is linked to the increasing intensity of typhoons from the ocean. A similar pattern of continuous decadal increase in SSTA in all months is followed by the South China Sea and the Philippine Sea except for the months of May, October, and November in the Philippine Sea and May, July October, and November in the South China Sea where the current decade (2007–2016) SSTA changes were less than the previous decade (1997–2006).

In summary, an increase in the temperature of the sea surface is one of the crucial reasons for increasing the strength of typhoons in the ocean regions that create typhoons for Taiwan. It is shown by month-wise, ENSO phase-wise, year-wise, decade-wise, and 5-year-wise climatological analyses (Tu et al., 2009, 2011; Mei and Xie, 2016).

### 5.8. *Typhoon strength inside Taiwan*

The current paper does not focus on assessing all typhoon parameters inside Taiwan as mentioned in this paper earlier as well. Yet to enhance the understanding of the typhoon scenario for Taiwan, two fundamental typhoon parameters (the maximum wind speed and the minimum pressure) are used to make maps as shown below (Fig. 17). Details of the method used are given in sub-section 4.6.

Fig. 17a and b reveal that no portion of Taiwan is free from the influence of typhoons although large contrast in the strength of typhoons is seen within different potions of the country. Fig. 17a and b shows that

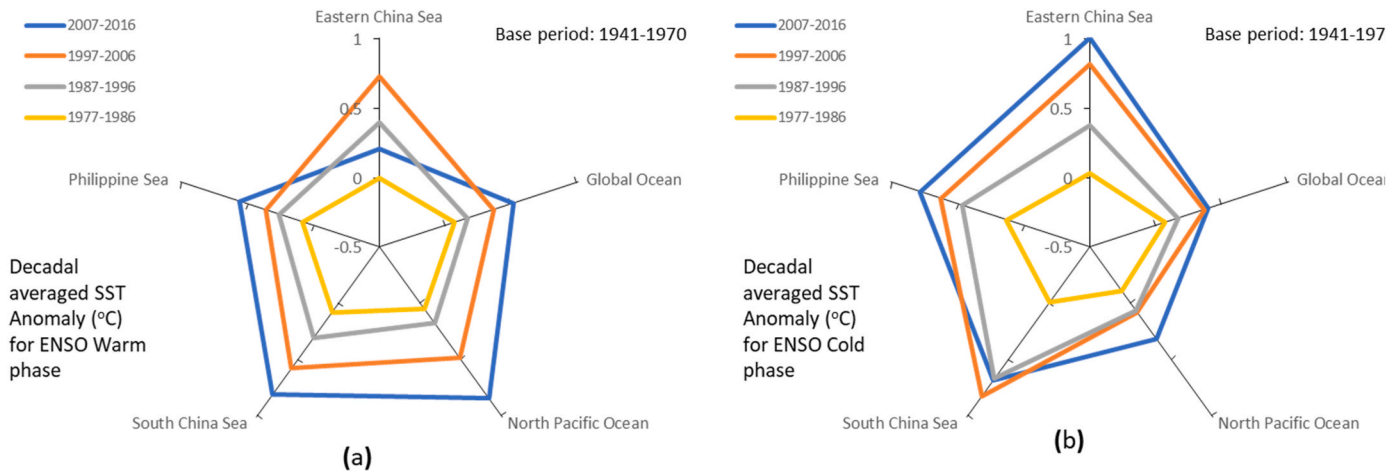


**Fig. 15.** The decadal variation in ENSO phases based on averaged SSTA in various oceans. Note here that for each ENSO phase and each decade, the same base years averaged months data is used for consistency.

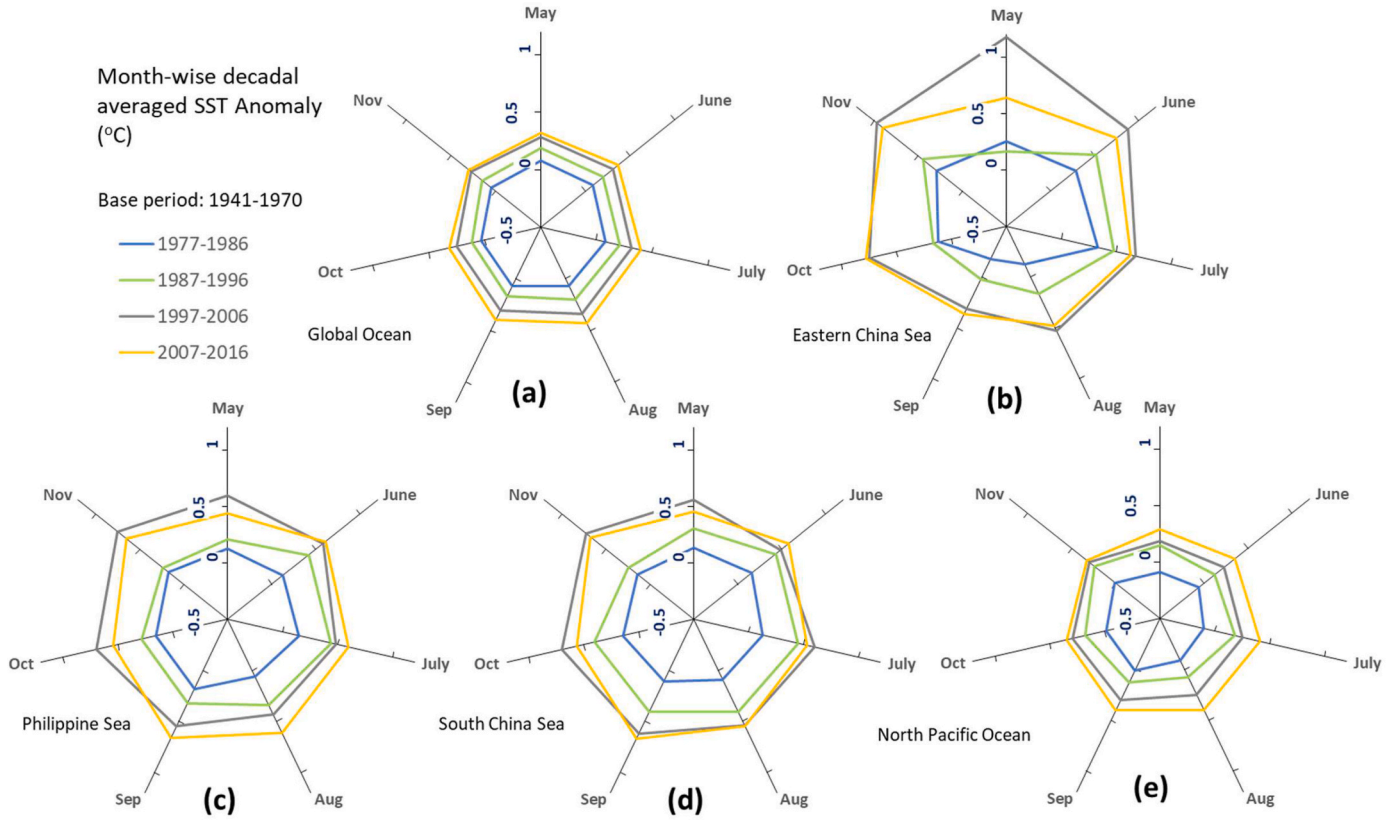


**Fig. 16.** Month-wise decadal averaged SST Anomaly (°C) in study oceans including global ocean during 1977–2016.

the strength of typhoons is maximum (red color) at the Eastern middle side of the country. Three components are contributing to this effect. First, the majority of typhoons enter Taiwan from the East side (around 53%) so as they carry more intensity (on average 949.3 hPa) in comparison to typhoons entering from the West or South; (2) The two major typhoon pathways (typhoon pathways 1 and 3) literally pass through mid-portion of the Eastern side of Taiwan accounting for almost 34% of all typhoons to Taiwan during the study period; and (3) The high mountain ranges extending from the north to the south as shown in Fig. 17c, works as a barrier for the typhoons to reduce their strength further in the Western parts of the country. Elevation plays a key role in setting the level of impact of typhoons in any area (Chi et al., 2015). In contrast, typhoons coming from the West (West-south) to Taiwan, with pathways 5, 6, and 10 (Fig. 5), are the weakest with an average strength of 969.9 hPa during the whole study period. The influenced areas by them are shown by the blue color in Fig. 17a and b. Also, this area is mostly having plain land and lacks any major mountain (Fig. 17c). Hence, it is observed that the results provided by this paper are completely in the sink with the typhoons' strength inside Taiwan. Fig. 17 is naturally suitable to validate the results found in this paper in terms of the frequency and strength of typhoons that hit Taiwan following various pathways. This kind of investigation is very crucial for a country that has been influenced by typhoons for long with increasing strength in recent years already putting further challenges for the

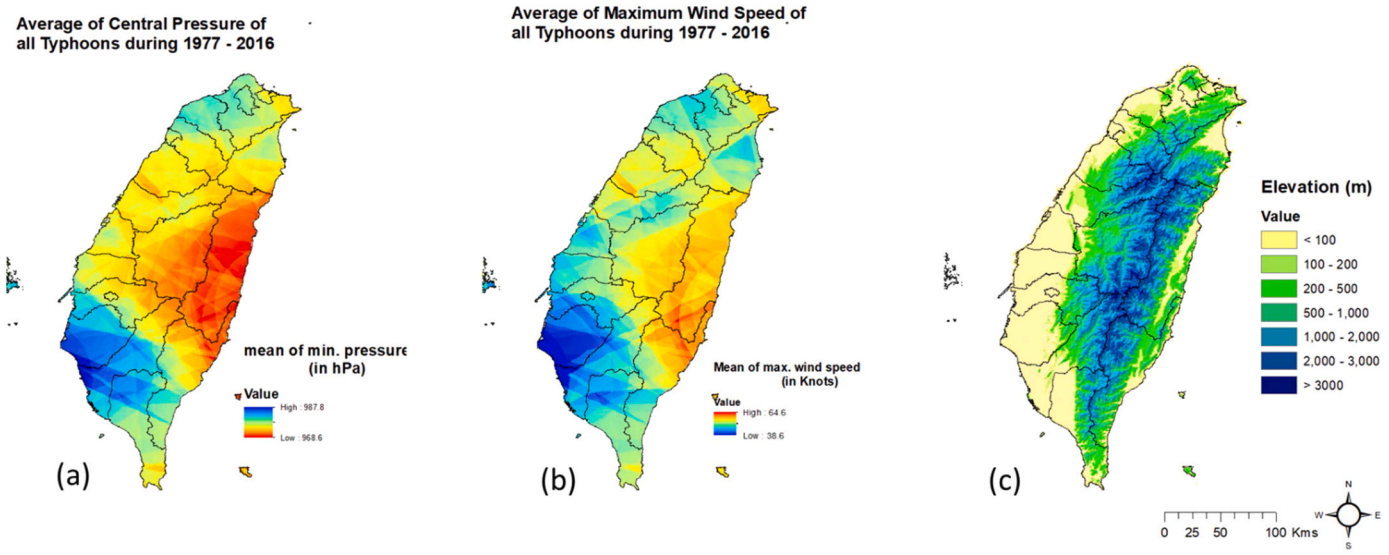


**Fig. 17.** (a) Average central pressure, and (b) average maximum wind speed maps based on all 77 typhoons from 1977 to 2016, while, (c) shows the elevation within entire Taiwan.

disaster management agencies of the country to mitigate the impacts of typhoons within the country (Pandey et al., 2021).

## 6. Conclusions

The current paper analyzed the tracks and cyclogenesis locations in different oceans quantitatively and also climatologically for all typhoons that hit Taiwan and appeared during the typhoon season of May to November from 1977 to 2016. The key conclusions are summarized below:

(1) Typhoons that cross Taiwan from around the center, after their first crossing the Eastern mountain range (extended in the North-South direction) from almost mid (typhoon pathway 1), are maximum in frequency (tie with typhoon pathway 2) and strength among all other typhoons reach to Taiwan. These typhoons enter Taiwan from the East (literally the East-south) direction. The majority of typhoons (>half, 53%) strike Taiwan from the East. They are on average stronger than the typhoons coming from the other different directions. The least (22%) number of typhoons come from the West to Taiwan, but surprisingly they survive on average the longest hours with maximum curves in their tracks than the typhoons coming from other different directions.

(2) The Philippine Sea dominates in the frequency of typhoons to Taiwan, whereas the North Pacific Ocean dominates in maximum strength and survival hours of typhoons. In comparison, the South China Sea dominates in maximum track sinuosity and has the highest number of weak typhoons. Besides, the South China Sea also has the second-longest survival rate of typhoons after the North Pacific Ocean. The Eastern China Sea has the lowest number of typhoons reaching Taiwan and has only been active in the recent two decades (1997–2016).

(3) The North Pacific Ocean is the outermost of Taiwan among all four Seas. Hence, typhoons coming to Taiwan from the North Pacific Ocean are supposed to survive the longest hours with maximum sinuosity in their tracks and strength as per previous studies (Pandey and Liou, 2020a). The above statement is found true in terms of survival hours and strength only. Surprisingly, the South China Sea despite being one of the borderings to Taiwan possesses maximum sinuous tracks with the second-longest surviving typhoons, although the majority of typhoons are weak. This surprising phenomenon of the South China Sea is contributed by the existence of the maximum number of the West directional typhoons, where the West directional typhoons on average survive the longest than any other directional typhoons to Taiwan.

(4) The warm phase of ENSO caused around 26% more cyclogenesis than the cold phase. The cyclogenesis during the warm phase of ENSO is also detected gradually rising over the last 4 decades.

(5) Statistical investigation on the relationships between various typhoon related parameters (SI, duration, distance covered, and minimum pressure) using Fisher's Exact and Two-sided chi-square ($\chi 2$) tests reveals vital information that the sinuous nature of tracks of typhoons is more responsible for the longer survival of typhoons ($r = 0.67$) than its strength.

(6) The 10-yearly (Decadal), 5-yearly, yearly, ENSO phase-wise, and month-wise climatological analyses by measuring the SSTA for the whole typhoon season (May–November) over the entire global ocean, the North Pacific Ocean, the Philippine Sea, the South China sea, and the Eastern China Sea reveal that there is a 0.4–0.7 °C rise in SST in all above oceans in the last 4 decades (1977–2016) in comparison to base years (1941–1970). The results are consistent with global warming leading to the increasing strength of typhoons that reach Taiwan. The Eastern China Sea has shown the maximum SST change during the last 4 decades, potentially due to its more closeness to the land areas of China and Japan along with its small overall size, which needs further investigation for surety. The role of El-Niño epochs is found very crucial for the large SSTA variations during typhoon season.

(7) There is an approximately 35% crucial increase in the decadal-averaged strengths of typhoons from 1977 to 1986 to 2007–2016 caused by 0.4–0.7 °C rise in Sea Surface Temperature (SST) in all oceans that originate typhoons of interest. An average of 1.9 typhoons per year hit Taiwan in the last 40 years of the study period (1977–2016).

This paper emphasizes the importance of studying the nature of tracks and cyclogenesis locations of typhoons for a particular country to understand the long-term and recent quick varying patterns in the typhoon parameters due to global warming to enhance appropriate planning to mitigate the impact of typhoons on the country.

## Authors contribution

Conceptualization, R.S.P. and Y.A.L.; data curation, R.S.P. and Y.A.L.; methodology and formal analysis, R.S.P.; writing—original draft preparation, R.S.P. and Y.A.L.; writing—review and editing, Y.A.L.

## Data availability statement

All Sea Surface Temperature Anomaly (SSTA) data with a time frame of 1977–2016 and base years 1941–1970 is available online on the Mendeley data repository and accessible through the link https://doi.org/10.17632/4ynzr5n3s6.1 (Pandey and Liou, 2020b). While the same time period all typhoons' track data is available online on the Mendeley data repository and accessible through the link https://doi.org/10.17632/3927f6gm72.1 (Pandey and Liou, 2020c).

## Declaration of competing interest

The authors declare that they have no known competing financial interests or personal relationships that could have appeared to influence the work reported in this paper.

## Acknowledgements

Two anonymous referees are thanked for providing constructive comments on the original manuscript submission. This work was supported by the Ministry of Science and Technology under Grant MOST 110-2634-F-008-008 and Grant MOST 110-2111-M-008-008.

## References

Astier, N., Plu, M., Claud, C., 2015. Association between tropical cyclone activity in the Southwest Indian ocean and El Nino southern oscillation. Atmos. Sci. Lett. 16, 506–511. https://doi.org/10.1002/asl.589.

Chang, C.T., Vadeboncoeur, M.A., Lin, T.C., 2018. Resistance and resilience of social–ecological systems to recurrent typhoon disturbance on a subtropical island: Taiwan. Ecosphere 9 (1), e02071. https://doi.org/10.1002/ecs2.2071.

Chi, C.H., McEwan, R.W., Chang, C.T., Zheng, C., Yang, Z., Chiang, J.M., Lin, T.C., 2015. Typhoon disturbance mediates elevational patterns of forest structure, but not species diversity, in humid monsoon Asia. Ecosystems 18, 1410–1423. https://doi.org/10.1007/s10021-015-9908-3.

Dvorak, V.F., 1972. A technique for the analysis and forecasting for tropical cyclone intensities from satellite pictures. NOAA Tech. Memo. NESDIS 36, 15. https://repository.library.noaa.gov/view/noaa/18546.

Dvorak, V.F., 1973. A technique for the analysis and forecasting for tropical cyclone intensities from satellite pictures. NOAA Tech. Memo. NESDIS 45, 19. https://repository.library.noaa.gov/view/noaa/18546.

Emanuel, K., 2005. Increasing Destructiveness of TCs over the past 30 years. Nature 436 (7051), 686–688. https://doi.org/10.1038/nature03906.

Hornyak, T., 2020. Typhoons Getting Stronger, Making Landfall More Often, vol. 101. Eos Transactions American Geophysical Union. https://doi.org/10.1029/2020EO147989 on. (Accessed 12 August 2020).

Hsu, S.A., Yana, Z., 1998. A Note on the radius of maximum winds for hurricanes. J. Coast Res. 12 (2), 667–668. JSTOR 4298820.

International Civil Aviation Organization, 1993. Manual of the ICAO Standard Atmosphere, third ed. In: Doc 7488-CD, ISBN 92-9194-004-6.

International Hydrographic Organization, 1953. Limits of Oceans and Seas, third ed. *(PDF)*. https://epic.awi.de/id/eprint/29772/1/IHO1953a.pdf.

James, H., Makiko, S., Reto, R., Ken, L., David, W.L., Martin, M.E., 2006. Global temperature change. Proc. Natl. Acad. Sci. U.S.A. 103 (39), 14288–14293. https://doi.org/10.1073/pnas.0606291103.

Janapati, J., Seela, B.K., Lin, P., Wang, P.K., Kumar, U., 2019. An assessment of tropical cyclones rainfall erosivity for Taiwan. Sci. Rep. 9, 15862 https://doi.org/10.1038/s41598-019-52028-5.

Jien, J.Y., Gough, W.A., Butler, K., 2015. The influence of El Niño–Southern oscillation on tropical cyclone activity in the eastern North Pacific basin. J. Clim. 28, 2459–2474. https://doi.org/10.1175/JCLI-D-14-00248.1.

Kim, J.S., Yoon, S.K., Oh, S.M., Moon, Y.I., 2015. Changes in typhoon activities and regional precipitation variability over the Korean Peninsula according to different phases of El Niño. Adv. Meteorol. 1687–9309. https://doi.org/10.1155/2015/983268, 2015.

Knutson, T.R., Sirutis, J.J., Garner, S.T., Vecchi, G.A., Held, I.M., 2008. Simulated reduction in Atlantic hurricane frequency under twenty–first–century warming conditions. Nat. Geosci. 1, 359–364. https://doi.org/10.1038/ngeo202.

Kornei, K., 2020. Storms Interact but Rarely Merge into Bigger Tempests, vol. 101. Eos Transactions American Geophysical Union. https://doi.org/10.1029/2020EO148366 on. (Accessed 26 August 2020).

Lee, Y.S., Liou, Y.A., Liu, J.C., Chiang, C.T., Yeh, K.D., 2017. Formation of winter Supertyphoons Haiyan (2013) and Hagupit (2014) through interactions with cold fronts as observed by multifunctional transport satellite. IEEE Trans. Geosci. Rem. Sens. 55 (7), 3800–3809. https://doi.org/10.1109/TGRS.2017.2680418.

Liou, Y.A., Liu, J.C., Liu, C.P., Liu, C.C., 2018. Season–dependent distributions and profiles of seven Super–Typhoons (2014) in the Northwestern Pacific Ocean from satellite cloud images. IEEE Trans. Geosci. Rem. Sens. 56 (5), 2949–2957. https://doi.org/10.1109/TGRS.2017.2787606.

Liou, Y.A., Pandey, R.S., 2020. Interactions between typhoons Parma and Melor. North West Pacific Ocean. Weather and Climate Extremes 29. https://doi.org/10.1016/j.wace.2020.100272, 2009.

Liou, Y.A., Liu, J.C., Wu, M.X., Lee, Y.J., Cheng, C.H., Kuei, C.P., Hong, R.M., 2016. Generalized empirical formulas of threshold distance to characterize cyclone–cyclone interactions. IEEE Trans. Geosci. Rem. Sens. 54 (6), 3502–3512. https://doi.org/10.1109/TGRS.2016.2519538.

Mei, W., Xie, S.P., 2016. Intensification of landfalling typhoons over the northwest Pacific since the late 1970s. Nat. Geosci. 9, 753–757. https://doi.org/10.1038/ngeo2792.

Mei, W., Xie, S.P., Primeau, F., McWilliams, J.C., Pasquero, C., 2015. Northwestern Pacific typhoon intensity controlled by changes in ocean temperatures. Sci. Adv. 1 (4), e1500014 https://doi.org/10.1126/sciadv.1500014.

Morakot Post-Disaster Reconstruction Council Report, 2010. In: Yang, H.H., Chen, S.Y., Chien, S.Y., Li, W.S. (Eds.), Forensic Investigation of Typhoon Morakot Disaster: Nansalu and Daniao Village Case Study (PDF), p. 2 (May 2014). http://www.irdrinternational.org/wp-content/uploads/2013/04/Morakot-Report.pdf. (Accessed 24 July 2020).

Nguyen, K.A., Liou, Y.A., Terry, J.P., 2019. Vulnerability of Vietnam to typhoons: a spatial assessment based on hazards, exposure and adaptive capacity. Sci. Total Environ. 682, 31–46. https://doi.org/10.1016/j.scitotenv.2019.04.069.

NOAA Hurricane Research Division, 2010. http://www.aoml.noaa.gov/hrd/tcfaq/E25.html. (Accessed 26 October 2019).

Pandey, R.S., Liou, Y.A., 2020a. Decadal behaviors of tropical storm tracks in the North West Pacific Ocean. Atmos. Res. 246 https://doi.org/10.1016/j.atmosres.2020.105143.

Pandey, R.S., Liou, Y.A., 2020c. Refined and improved tropical storm 6-hourly data and track sinuosity measurements for the North West Pacific basin during 1977-2016. Mendeley Data, *v1*. https://doi.org/10.17632/3927f6gm72.1.

Pandey, R.S., Liou, Y.A., 2020b. Yearly, 5-yearly, and decadal Sea surface temperature (SST) and SST anomaly (SSTA) data averaged over the whole typhoon season (May-November) over the entire global ocean, north Pacific Ocean, Philippine sea, south China sea, and eastern China sea. Mendeley Data, V1. https://doi.org/10.17632/4ynzr5n3s6.1.

Pandey, R.S., Liou, Y.A., Liu, J.C., 2021. Season-dependent Variability and Influential Environmental Factors of Super-typhoons in the Northwest Pacific Basin during 2013-2017, vol. 31. Weather and Climate Extremes. https://doi.org/10.1016/j.wace.2021.100307.

Peduzzi, P., Chatenoux, B., Dao, H., De Bono, A., Herold, C., Kossin, J., Mouton, F., Nordbeck, O., 2012. Global trends in tropical cyclone risk. Nat. Clim. Change 2, 289–294. https://doi.org/10.1038/nclimate1410.

Reynolds, R.W., Rayner, A.N., Smith, T.M., Stokes, D.C., Wang, W., 2002. An improved in situ and satellite SST analysis for climate. J. Clim. 15, 1609–1625. https://doi.org/10.1175/1520-0442(2002)015<1609:AIISAS>2.0.CO;2.

Schreck, C.J., Knapp, K.R., Kossin, J.P., 2014. The impact of best track discrepancies on global tropical cyclone climatologies using IBTrACS. Mon. Weather Rev. 142, 3881–3899. https://doi.org/10.1175/MWR-D-14-00021.1.

Smith, R.K., 1980. Tropical cyclone eye dynamics. J. Atmos. Sci. 37 (6), 1227–1232. https://doi.org/10.1175/1520-0469(1980)037<1227:TCED>2.0.CO;2.

Song, J.J., Wang, Y., Wu, L., 2010. Trend discrepancies among three best track data sets of western North Pacific tropical cyclones. J. Geophys. Res. 115, D12128. https://doi.org/10.1029/2009JD013058.

Terry, J.P., Gienko, G., 2011. Developing a new sinuosity index for cyclone tracks in the tropical South Pacific. Nat. Hazards 59, 1161–1174. https://doi.org/10.1007/s11069-011-9827-3.

Terry, J.P., Gienko, G., 2018. Quantitative observations on tropical cyclone tracks in the Arabian Sea. Theor. Appl. Climatol. 135, 1413–1421. https://doi.org/10.1007/s00704-018-2445-1.

Terry, J.P., Kim, I.K., 2015. Morphometric analysis of tropical storm and hurricane tracks in the North Atlantic basin using a sinuosity–based approach. Int. J. Climatol. 35, 923–934. https://doi.org/10.1002/joc.4027.

Terry, J.P., Kim, I.K., Jolivet, S., 2013. Sinuosity of tropical cyclone tracks in the South west Indian Ocean: Spatio–temporal patterns and relationships with fundamental storm attributes. Appl. Geogr. 45, 29–40. https://doi.org/10.1016/j.apgeog.2013.08.006.

Tu, J.Y., Chou, C., Chu, P.S., 2009. The abrupt shift of typhoon activity in the vicinity of Taiwan and its association with western North Pacific East Asian climate change. J. Clim. 22, 3617–3628. https://doi.org/10.1175/2009JCLI2411.1.

Tu, J.Y., Chou, C., Huang, P., Huang, R., 2011. An abrupt increase of intense typhoons over the western North Pacifc in early summer. Environ. Res. Lett. 6 (3), 034013 https://doi.org/10.1088/1748-9326/6/3/034013.

Webster, P.J., Holland, G.J., Curry, J.A., Chang, H.R., 2005. Changes in TC number, duration, and intensity in a warming environment. Science 309 (5742), 1844–1846. https://doi.org/10.1126/science.1121564.

Wolter, K., Timlin, M.S., 2011. El Niño/Southern Oscillation behaviour since 1871 as diagnosed in an extended multivariate ENSO index (MEI.ext). Int. J. Climatol. 31, 1074–1087. https://doi.org/10.1002/joc.2336.

Zhang, Q., Wu, L., Liu, Q., 2009. Tropical cyclone damages in China 1983–2006. Bull. Am. Meteorol. Soc. 90, 489–496. https://doi.org/10.1175/2008BAMS2631.1.

Zhao, H., Wu, L., Wang, R., 2014. Decadal variations of intense tropical cyclones over the western North Pacific during 1948–2010. Adv. Atmos. Sci. 31, 57–65. https://doi.org/10.1007/s00376-013-3011-5.